

Towards precision cosmology with Voids \times CMB correlations (I)

Roman-Agora mock catalogs and pipeline validation

Mar Pérez Sar^{1,2*}, Carlos Hernández Monteagudo¹, András Kovács^{3,4}, and Alice Pisani^{5,6}

¹ Instituto de Astrofísica de Canarias, Calle Vía Láctea s/n, E-38205, La Laguna, Tenerife, Spain

² Departamento de Astrofísica, Universidad de La Laguna, E-38206, La Laguna, Tenerife, Spain

³ MTA–CSFK Lendület “Momentum” Large-Scale Structure (LSS) Research Group, Konkoly Thege Miklós út 15-17, H-1121 Budapest, Hungary

⁴ Konkoly Observatory, HUN-REN Research Centre for Astronomy and Earth Sciences, Budapest, Hungary

⁵ CPPM, Aix-Marseille Université, CNRS/IN2P3, Marseille, France

⁶ Department of Astrophysical Sciences, Peyton Hall, Princeton University, Princeton, NJ 08544, USA

Received xxx, 2024; accepted xxx, 2024

ABSTRACT

We construct and validate a set of multi-purpose mock galaxy catalogs designed to capture, to different degrees of accuracy, the main characteristics of the Nancy Grace *Roman* Space Telescope survey. These catalogs provide a foundation for void statistics and various Cosmic Microwave Background (CMB) cross-correlation analyses.

Our approach differs from traditional halo occupation or abundance matching methods by directly translating a reference mock catalog—containing basic properties of the host halos—into a new simulation (in our case Agora). This technique, which we call *analog matching*, assigns a halo counterpart in the new simulation to each reference galaxy through a nearest-neighbor search in a multi-dimensional parameter space. This space can include halo mass, environmental measures and other galaxy-specific attributes. By varying the composition of this parameter vector, we can generate catalogues of differing complexity and conduct systematic tests to examine the influence of modelling choices on LSS statistics.

We find that analog matching based on halo mass alone, or halo mass and galaxy-type indicators, successfully reproduces the expected *Roman* emission-line galaxy statistics. We also show that reproducing two-dimensional galaxy clustering does not guarantee consistent void properties. Our results highlight the importance of matching void statistics for improved mock accuracy, and demonstrate that measuring voids provides independent and sensitive constraints on galaxy-halo connections beyond the matter power spectrum. An important by-product of our setup is that it is fully general and can be applied to any combination of simulation and reference catalogue, provided that the desired parameter space for both is specified. The resulting *Roman*-Agora mock catalogs offer a versatile resource for LSS \times CMB studies and a benchmark for assessing the impact of mock accuracy on cosmological observables.

Key words. Cosmology: Large-scale structure - Cosmic microwave background - Mock catalogs - Cosmic voids

1. Introduction

From our tiny blue point of view, we have expanded our understanding of the Universe by collecting vast datasets across the electromagnetic spectrum and cosmic history, and by interpreting them through theoretical models and simulations. These efforts have tested and refined our standard cosmological model, the Λ cold dark matter model (Λ CDM), which—with only six parameters and assuming general relativity and linear perturbations around a homogeneous and isotropic background—successfully describes most observations in a wide range of scales. Yet, its main ingredients, dark matter and dark energy, remain unknown, and as measurements and analysis techniques improve, subtle but persistent tensions have emerged, pointing either to unaccounted systematic effects or to new physics beyond our current understanding (Abdalla et al. 2022; Perivolaropoulos & Skara 2022; Peebles 2022; Efstathiou 2025).

Cross-correlating independent cosmological probes has become an essential strategy to address these tensions. Joint analyses exploit the complementary sensitivities of different observables, break degeneracies between cosmological and astrophys-

ical parameters, mitigate systematics errors that are unique to each individual dataset, and enhance the overall signal-to-noise of measurements that would otherwise remain undetectable (Ho et al. 2008; Hirata et al. 2008; Pearson & Zahn 2014; Nicola et al. 2016; Omori et al. 2023; Chang et al. 2023; Abbott et al. 2023).

The cross-correlation between the Cosmic Microwave Background (CMB) and the Large-Scale Structure (LSS) is particularly powerful. As CMB photons travel from the last scattering surface to us, their trajectories and energies are continuously perturbed by the evolving matter distribution via gravitational potentials—giving rise to gravitational lensing (Lewis & Challinor (2006), and the Sachs-Wolfe, SW, and integrated Sachs-Wolfe, ISW, effects Sachs & Wolfe (1967))—or via scattering off free electrons (through the so-called kinetic (kSZ) and thermal (tSZ) Sunyaev-Zel'dovich effects (Sunyaev & Zel'dovich 1980, 1972)), neutral hydrogen atoms (aka Rayleigh scattering, Basu et al. 2004; Lewis 2013), and even metallic and ionic species via (sub-) millimeter fine-structure transitions (Basu et al. 2004; Hernández-Monteagudo et al. 2006, 2007). These LSS-induced distortions reprocess the original CMB signal, imprinting late-time information about the growth of struc-

* perezsarmar@gmail.com

ture and the geometry of the Universe. The resulting CMB \times LSS signals provide sensitive constraints on parameters including the matter density (Ω_m), clustering amplitude (σ_8), neutrino masses, and dark energy (Chen et al. 2021; Krolewski et al. 2021; Shaikh et al. 2024), while also detecting important systematic effects, such as the contamination of CMB lensing reconstructions by thermal SZ foregrounds and other higher-order LSS correlations which can bias the cosmological inference if not accounted for (Troxel & Ishak 2014).

For interpreting and extracting cosmological information from the CMB \times LSS measurements, realistic simulations are fundamental. Although analytical and semi-analytical models exist, they rely on simplifying assumptions that often break down in the non-linear regime and under realistic observational conditions. Simulations, therefore, provide the only framework capable of capturing the non-linear evolution of structure and the correlated physics that shape these observables. They allow us to model structure formation self-consistently, test and validate analysis pipelines, estimate statistical uncertainties and covariances, and identify potential systematic biases.

Building simulations that coherently include both CMB and LSS observables is, however, technically demanding. LSS tracers require high mass and spatial resolution to resolve small-scale structures, while CMB observables demand very large volumes to capture long-wavelength modes and line-of-sight projections. Additionally, subtle interdependences between different signals —namely CMB lensing, the Sunyaev-Zel'dovich effects, and the Cosmic Infrared Background (CIB)— must be captured accurately, as inconsistencies in modeling these relationships can bias cross-correlation measurements. Meeting all these requirements simultaneously leads to extreme computational and storage demands, often making it infeasible to generate many independent realizations.

Some examples of simulations that try to overcome these challenges are WEBSKY (Stein et al. 2020), DEMNUNI (Castorina et al. 2015; Carbone et al. 2016), AGORA (Omori 2024), GOWER STREET (Jeffrey et al. 2025), and HALFDOMe (Bayer et al. 2025), each adopting different compromises between resolution, number of realizations and cosmological coverage. Despite their specific trade-offs, all these simulations are highly valuable for cross-correlation studies and the optimal choice depends on the scientific application.

The last step, once a simulation is selected, is to make it suitable for cosmological analysis by tailoring its data products to match the specifications of the target survey. For the CMB-related outputs —including lensing, ISW, kSZ, tSZ, and CIB maps — only limited processing is required. These maps are typically adjusted by applying the survey mask or beam, adding noise realizations consistent with the instrumental sensitivity, and, if necessary, applying small multiplicative calibrations (typically at the few-percent level) to match the observed power spectra. Their validation is performed statistically, through comparisons of auto- and cross-power spectra with theoretical predictions (for example, from CAMB¹) and with existing measurements from experiments such as *Planck* (Planck Collaboration et al. 2014, 2016a, 2020), the Atacama Cosmology Telescope (ACT) (Das et al. 2011; Sherwin et al. 2017), or the South Pole Telescope (SPT) (Story et al. 2015; Wu et al. 2019), to ensure that they reproduce both the amplitude and scale dependence of the true sky signal.

In contrast, the LSS products —which at this stage describe only the dark matter distribution and its associated halos— re-

quire more extensive adaptation to emulate the galaxy surveys. Halos must be populated with galaxies using empirical or semi-analytic prescriptions that account for the survey's geometry, selection function, and galaxy bias (Somerville & Davé 2015; Wechsler & Tinker 2018). This bias captures the complex mapping shaped by baryonic processes, local environment, and the assembly history of halos which modulates the resulting galaxy clustering relative to the underlying dark matter.

Typically, mock catalogs are validated from the galaxy clustering perspective —ensuring that they reproduce the one- and two-point statistics of the target survey— but they are rarely tested with higher-order statistics, including bispectrum or voids. Cosmic voids form the low-density counterparts to the bright network that shape the cosmic web (Jøeuvre et al. 1978; Gregory & Thompson 1978; Pisani et al. 2019; Moresco et al. 2022). They arise in regions where matter is gravitationally drained towards surrounding overdensities, leading to interiors that reach only a fraction of the mean cosmic density. Importantly, voids extend across tens to hundreds of megaparsecs and occupy most of the Universe's volume, evolving in a regime where dynamics remain close to linear and baryonic effects are minimal (Lavaux & Wandelt 2012; Hamaus et al. 2014; Paillas et al. 2017). Their statistics encode higher-order correlations beyond traditional two-point clustering, providing additional means to evaluate how accurately mocks reproduce the full topology of the matter distribution (see e.g., Arsenov et al. 2025).

These properties make voids theoretically clean and highly sensitive cosmological probes, capable of constraining the expansion history, dark energy, and gravity primarily (Biswas et al. 2010; Bos et al. 2012; Pisani et al. 2015; Pollina et al. 2016; Hawken et al. 2017; Contarini et al. 2019a; Achitouv 2019; Correa et al. 2019; Nadathur et al. 2020; Paillas et al. 2021; Woodfinden et al. 2022; Pelliciari et al. 2023; Contarini et al. 2023; Mauland et al. 2023; Song et al. 2024; Fraser et al. 2025) through the void size function (Sheth & van de Weygaert 2004a; Furlanetto & Piran 2006; Jennings et al. 2013a; Pisani et al. 2015; Ronconi & Marulli 2017; Correa et al. 2021a; Contarini et al. 2023; Verza et al. 2024a; Fernández-García et al. 2025) and the void-galaxy cross-correlation function (with its distortions in redshift space) (Kaiser 1987; Alcock & Paczynski 1979; Lavaux & Wandelt 2012; Sutter et al. 2012; Pisani et al. 2014; Cai et al. 2016; Mao et al. 2017; Nadathur et al. 2019b; Aubert et al. 2022; Correa et al. 2022a; Hamaus et al. 2022; Woodfinden et al. 2022; Radinović et al. 2023; Verza et al. 2024b; Degni et al. 2025; Schuster et al. 2025).

In this work, we construct and validate a set of multi-purpose mock galaxy catalogs of varying levels of fidelity designed to capture, to different degrees, the main characteristics of the Nancy Grace *Roman* Space Telescope survey² (Spergel et al. 2015a), as a foundation for void statistic and various CMB cross-correlation analyses.

For this purpose, we choose the AGORA simulation (Omori 2024) since its mass and spatial resolution is sufficient for resolving the low-mass halos that host emission-line galaxies (ELGs), but also coherently includes secondary CMB anisotropy maps and astrophysical foregrounds.

In general, these qualities make AGORA particularly suitable for modeling the *Roman* survey, whose redshift coverage ($0.8 \leq z \leq 2$) is comparable with other modern cosmology missions such as *Euclid* (Laureijs et al. 2011) and the Dark Energy Spectroscopic Instrument (DESI) (DESI Collaboration et al. 2016). *Roman*'s depth and area will, however, provide a finer angular

¹ <https://camb.readthedocs.io/>

² <https://roman.gsfc.nasa.gov/>

resolution and a higher sampling density for accessing smaller scales, also offering an interesting point of view for detailed analyses of cosmic voids, which so far have been investigated in wide-areas and sparser galaxy datasets.

This *Roman*-AGORA mock framework offers a versatile tool for the community, enabling not only void analyses but also a broad range of future LSS-CMB cross-correlation studies, including 5 \times 2pt, tSZ, and kSZ measurements. While this paper focuses on describing and validating the mock catalogs themselves, a companion work will use these data products to investigate how different methodological choices—such as mock construction, void definitions, stacking techniques, and CMB map treatments—impact the Void \times CMB lensing signal and its forecasted detectability with *Roman* and upcoming CMB surveys.

The paper is organized as follows. In Section 2 we describe the data employed in this study. In Section 3, we present the methodology and discuss its limitations. Section 4 contains the results and discussion, and Section 5 concludes with a summary of our main findings.

2. Datasets

2.1. Roman Space Telescope

The Nancy Grace *Roman* Space Telescope (hereafter *Roman*) is a NASA observatory planned to be launched in late 2026 and designed to shape the future of astrophysics through pioneering research on dark energy, exoplanets, and infrared astronomy (Green et al. 2012; Spergel et al. 2015b; Observations Time Allocation Committee & Community Survey Definition Committees 2025). It shares considerable similarities with the Hubble Space Telescope, since its primary mirror has the same size (2.4 meters of diameter). However, its field of view is 100 times larger, allowing it to survey large areas of the sky with unprecedented detail and less observing time (1000 times faster than Hubble).

The telescope’s spectroscopy and imaging will operate in the near-infrared and visible wavelengths (only imaging) measuring millions of Emission-Line Galaxies (ELGs) as tracers of the underlying matter distribution. ELGs, identified through strong nebular emission lines such as H α , [OIII], and [OII], arise primarily from active star formation and, to a lesser extent, AGN activity, allowing precise spectroscopic redshift measurements (Gonzalez-Perez et al. 2020). The High Latitude Wide Area Survey (HLWAS) is the most relevant *Roman* program for this work, combining imaging and spectroscopy to produce a 3-dimensional map of galaxies.

The expected outcome of *Roman*, predicted from reference catalogs in the literature is a total of 14.2 million H α redshifts, 3.6 million [OIII] redshifts, and 1.3 million [OII] redshifts, with 11 million objects at $z > 1$ and 1.7 million at $z > 2$. Accurate redshift determination ideally requires the detection of two emission lines; when this is not possible, complementary imaging is necessary to help confirm the emission lines and to separate overlapping spectra. The grism’s wavelength range (1–1.9 μ m) ensures reliable detection of H α (0.656 μ m) and [OIII] (0.501 μ m) for redshifts between $1.1 < z < 1.9$, and [OIII] and [OII] (0.373 μ m) for $1.8 < z < 2.8$.

A multi-tier survey design is proposed for *Roman* (see Observations Time Allocation Committee & Community Survey Definition Committees (2025)), consisting of a 2415 deg^2 medium tier, an additional 2700 deg^2 wide tier, and a 19.2 deg^2 deep tier, together covering 5100 deg^2 in 520 days³.

³ The spectroscopic sources will come only for the deep and medium tiers space, i.e. $\sim 2415 \text{ deg}^2$.

2.1.1. Roman mock catalogs

To optimize the survey strategies and forecast its scientific outcome, several mock catalogs have been presented in the literature simulating *Roman*’s performance, although none incorporate coherent CMB maps attached to them. For example, Wang et al. (2022) forecasts constraints from baryon acoustic oscillations and redshift space distortions, while Verza et al. (2024c) study *Roman*’s constraining power from the void size function and the void-galaxy cross-correlation function.

The existing *Roman* mock catalog that we aim to replicate in this work is presented in Zhai et al. (2021)⁴. It was created using a semi-analytical galaxy formation model (SAM) GALACTICUS (Benson 2011), coupled with the N-body simulation UNIT (Chuang et al. 2019, see Table 1 for specifications). The SAM simulates the galaxy properties (such as stellar mass, star formation rate, metallicity, line luminosity) of the ELGs detected by the instrument in a $\sim 2000 \text{ deg}^2$ area, and calibrate them to match the observed H α luminosity function from the High-z Emission Line Survey (HiZELS, Geach et al. 2008; Sobral et al. 2009, 2013).

2.2. AGORA simulation

To generate a *Roman*-like mock catalog with associated secondary CMB anisotropy maps, we use the AGORA simulation by Omori (2024). It provides a single halo lightcone catalog with both CMB and LSS observables, and it includes CMB lensing convergence (κ), thermal and kinetic Sunyaev-Zel’dovich effects (tSZ/kSZ), the cosmic infrared background (CIB), radio sources, as well as galaxy density contrast and weak lensing maps.

The LSS component is based on a dark matter-only N-body simulation MULTIDARK PLANCK 2 (MDPL2) (Klypin et al. 2016)⁵, chosen for its extensive set of derived products that can be directly integrated with the simulation. Some examples are galaxy catalogs from semi-analytical models (Cora et al. 2018), studies of emission line galaxy populations (Alam et al. 2021), and intensity mapping predictions (Sato-Polito et al. 2023a). The specifications of MDPL2 are summarized in Table 1.

The lightcone is built by tiling the $1000 \text{ h}^{-1} \text{ Mpc}$ simulation box to fill the required volume, using periodic boundary conditions to maintain a continuous matter distribution across box edges. An observer is placed at the center, establishing the reference frame. From this point, spherical shells of 25 Mpc h^{-1} width are extracted radially, with halos and dark matter particles from the closest simulation snapshot projected onto a HEALPix grid at $N_{\text{side}} = 8192$ ($\sim 0.43 \text{ arcmin}$ resolution). To suppress artificial repetition along the line of sight, the shells are randomly rotated every 1000 Mpc h^{-1} (one full box length). These rotations are applied at a scale significantly larger than the correlation length of the density fluctuations and consistently across all fields (halo catalogs, density, and velocity) to ensure accurate cross-correlations without inducing unphysical discontinuities.

To generate the CMB κ map, the simulation adopts a multi-plane ray tracing approach, which follows light rays as they traverse successive spherical shells of the matter distribution. This method accurately captures cumulative and higher-order gravitational effects beyond the common Born approximation. The

⁴ <https://irsa.ipac.caltech.edu/data/theory/Roman/Zhai2021/>

⁵ Description of the simulation and various data products can be accessed at <https://www.cosmosim.org/metadata/MDPL2/>, with halo catalogues available at <http://halos.as.arizona.edu/simulations/MDPL2/hlists/>.

Simulation Year	General N-body parameters				Cosmology parameters				ROCKSTAR parameters		
	Size (h^{-1} Mpc)	Particles	$\text{res } m_p$ (h^{-1} M_\odot)	$\log M_h$ (h^{-1} M_\odot)	h	Ω_m	σ_8	n_s	Linking length (h^{-1} Mpc)	Min number of particles per halo	Force resolution (h^{-1} kpc)
UNIT (Roman) 2016 (2021)	1000	4096	$1.2 \cdot 10^9$	8.18	0.6774	0.3089	0.8147	0.9667	$0.2 L_{\text{box}}/N_c$	20	6
MDPL2 (Agora) 2017 (2022)	1000	3840	$1.5 \cdot 10^9$	11.01	0.6777	0.3071	0.8288 (0.818)	0.96	0.2	≥ 250	13 (high-z) 5 (low-z)

Table 1: Overview of the large-volume UNIT and MDPL2 simulations, which serve as the basis for the *Roman* reference catalog and the AGORA project. We compare general simulation parameters, adopted cosmology, and ROCKSTAR halo finder settings.

procedure divides the redshift range into two regimes: (i) For $z < 8.6$, the matter in each shell is converted into a gravitational potential. The first derivatives are computed to construct the local deflection field, $\alpha(\hat{\mathbf{n}}) = \nabla_\Omega \phi(\hat{\mathbf{n}})$, where ϕ is the lensing potential, a projection of the 3D gravitational potential Φ and the operator ∇_Ω denotes the *angular gradient* on the unit sphere, defined as $\nabla_\Omega = \hat{\theta} \frac{\partial}{\partial \theta} + \frac{\hat{\varphi}}{\sin \theta} \frac{\partial}{\partial \varphi}$, which measures directional derivatives with respect to angular coordinates (θ, φ) on the sky. The second derivatives are computed to define the optical tidal matrix $\Psi_{ij} = \nabla_{\Omega,i} \nabla_{\Omega,j} \phi(\hat{\mathbf{n}})$, which acts as a local magnification matrix encoding the convergence, shear, and rotation in that shell. Both fields are computed on a HEALPix (Górski et al. 2005)⁶ grid with $N_{\text{side}} = 16384$.

Using GRAYTRIX (Shirasaki et al. 2015), light rays are traced backward from $z = 0$ to $z = 8.6$ through successive lens planes of $25 h^{-1}$ Mpc thick. At each plane, the deflection field α updates the ray's direction which is then used for Ψ to update how the light bundle has been distorted (shear, convergence, rotation). The matrix Ψ iteratively propagates the lensing magnification matrix $\mathbf{A} = \mathbf{I} - \Psi$, capturing the cumulative distortions of the light bundle along the line of sight. From the final magnification matrix, \mathbf{A} , the CMB lensing convergence map is obtained like:

$$\kappa^{\text{low-z}}(\hat{\mathbf{n}}) = 1 - \frac{1}{2} \text{Tr}(\mathbf{A}) \quad (1)$$

The map is slightly smoothed to $N_{\text{side}} = 8192$ to optimize computational efficiency while retaining small-scale accuracy.

For $z > 8.6$, where the density field remains approximately linear and Gaussian, a Gaussian realization of the lensing potential is added, based on the theoretical power spectrum. An additional correction is applied at low multipoles ($\ell \leq 10$) to mitigate residual tiling artifacts.

$$\kappa^{\text{high-z}}(\hat{\mathbf{n}}) = -\frac{1}{2} \nabla_\Omega^2 \phi(\hat{\mathbf{n}}) \iff \kappa_{\ell m}^{\text{high-z}} = \frac{1}{2} \ell(\ell + 1) \phi_{\ell m}. \quad (2)$$

The final map will be the sum of both contributions:

$$\kappa^{\text{tot}}(\hat{\mathbf{n}}) = \kappa^{\text{low-z}}(\hat{\mathbf{n}}) + \kappa^{\text{high-z}}(\hat{\mathbf{n}}) \quad (3)$$

All the AGORA CMB maps, including CMB κ , are calibrated and validated against observational data from *Planck* (The Planck Collaboration 2006), SPT-SZ (Carlstrom et al. 2011), and SPTpol (Bleem et al. 2012), achieving sub-arcminute resolution and accurate statistics across $50 \lesssim \ell \lesssim 3000$. The LSS products (galaxy clustering and weak lensing) are similarly validated over $30 \lesssim \ell \lesssim 3000$ verifying that the simulation outputs are suitable for realistic cosmological studies.

Our analysis relies on the originally publicly released AGORA products. While these are no longer publicly available at the time of submission of this work, the project webpage⁷ indicates that updated versions are shared with collaborators.

2.2.1. Comparison between UNIT and MDPL2

Table 1 compares the source simulations behind our datasets, UNIT for the *Roman* catalog and MDPL2 for the AGORA simulation, across three categories: (i) general N-body parameters, (ii) cosmological parameters, and (iii) the ROCKSTAR halo finder configuration (Behroozi et al. 2013), with merger histories computed using CONSISTENT TREES⁸ in both cases.

General N-body parameters. The AGORA reference catalog from UNIT has a higher resolution: for the same $1 h^{-1}$ Gpc box, it uses 4096^3 particles compared to the 3840^3 of MDPL2. This leads to a finer particle mass resolution of $1.2 \times 10^9 h^{-1} M_\odot$ for UNIT, versus $1.5 \times 10^9 h^{-1} M_\odot$ for MDPL2. UNIT can resolve haloes down to $\log M_h \sim 8.2$, while MDPL2 reaches only $\log M_h \sim 11.0$, and this is due to the adoption of different particle thresholds at defining haloes (see below). To ensure consistent resolution across catalogs, we apply a halo mass cut to the *Roman* reference catalog to match the AGORA resolution, which results in the loss of 1.32% of the total galaxies. In the Appendix, we demonstrate how particle loss affects 3D and 2D voids and show that this cut has a minimal impact on our results.

Cosmological parameters. Both simulations adopt parameters consistent with (Planck Collaboration et al. 2016b), with only minor differences. Notably, while MDPL2 uses $\sigma_8 = 0.8288$, the AGORA products are generated with $\sigma_8 = 0.818$ to better match the amplitude of the matter power spectrum.

– ROCKSTAR parameters.

- Linking length:** defines the maximum distance at which particles are considered part of the same halo, expressed as a fraction of the mean inter-particle separation (commonly $b = 0.2$). UNIT scales this with resolution ($b = 0.2 L_{\text{box}}/N_c$ where L_{box} is the size of the box and N_c the number of cells or particles along one dimension of the simulation). MDPL2 uses a fixed $b = 0.2$, providing a standard, resolution-independent definition. The main consequence is that halo masses (and, in some cases, halo sizes) can differ slightly between the two simulations. This effect is most significant for low-mass halos but it will be negligible in our case for halos with $M_h > 10^{11} h^{-1} M_\odot$.
- Minimum particles per halo:** UNIT can have halos with as few as 20 particles, including very low-mass systems at the cost of increased noise and less reliable halo properties. In contrast, MDPL2 requires at least 250 particles per halo, so that all identified halos are well resolved and their internal properties are statistically robust, though excluding the low-mass population.
- Force resolution:** Gravitational forces are softened below a characteristic scale to prevent numerical instabilities.

⁶ HEALPix's URL site <http://healpix.sf.net>

⁷ <https://yomori.github.io/Agora/index.html>

⁸ <https://bitbucket.org/pbehroozi/consistent-trees/src/main/>

UNIT adopts a fixed softening length of $6 h^{-1}$ kpc across all redshifts to preserves a uniform resolution across the simulation, while MDPL2 uses a redshift-dependent softening, $13 h^{-1}$ kpc at high z and $5 h^{-1}$ kpc at low z so that halos are reliably detected at both early and late times. Again, the choice of softening primarily affects the smallest halos and their internal structure, particularly at low masses which will be excluded from our analysis.

Overall, the UNIT and MDPL2 simulations reflect different design priorities, particularly in their N-body and ROCKSTAR configurations: the purpose of UNIT is *completeness*, capturing small halos down to dwarf scales, while the goal of MDPL2 is *robustness*, focusing on well-resolved halos. Despite these differences, we make the two simulations compatible for our mock catalog construction by applying a minimum halo mass cut at the AGORA limit $M_h > 10^{11} h^{-1} M_\odot$ which can equalize their effective resolution. As we have mentioned, this minimum halo mass cut results in only a 1.32% loss in the *Roman* galaxy sample coming from UNIT, demonstrating that MDPL2 and consequently AGORA provides a reliable choice for our mocks without introducing significant incompleteness.

3. Methodology

In this section, we present the methodology used for constructing the *Roman* mock galaxy and void catalogs, based on the AGORA simulation.

3.1. State of the art in mock catalogs

As outlined in the introduction, mock galaxy catalogs are synthetic datasets simulating the universe's galaxy distribution, that play an essential role in modern large-scale structure analyses. Constructing these catalogs requires modeling the galaxy–halo connection, which links galaxies to the underlying dark matter distribution (Kaiser 1984; Bardeen et al. 1986; Mo & White 1996; Fry 1996; Tegmark & Peebles 1998). Halo abundance and clustering are primarily determined by cosmology and are well captured in (pure dark matter) N-body simulations. Nonetheless, mapping from halos to galaxies is significantly more complex, since this process is heavily influenced by baryonic physics that cannot be modeled trivially, such as gas cooling, star formation, and AGN and supernova feedback.

Galaxy–halo connections can be modeled with physics-based or empirical-based approaches, tuned to reproduce fundamental observational quantities. Physics-based methods capture galaxy formation from first principles and include **hydrodynamical simulations**, which model the co-evolution of dark matter and baryons simultaneously, solving the fundamental equations of gravity, hydrodynamics, and thermodynamics (Dubois et al. 2014a; Schaller et al. 2015; Dolag et al. 2016; McCarthy et al. 2017; Springel et al. 2018; Villaescusa-Navarro et al. 2021; Schaye et al. 2023), and **semi-analytic models (SAMs)**, which use the information of halo merger trees from N-body simulations and simplified analytic recipes to model the relevant baryonic processes (Somerville & Davé 2015; Dubois et al. 2014b; Perez et al. 2023; Bower et al. 2006; Behroozi et al. 2019; Benson 2011). On the other hand, empirical methods derive statistical galaxy - halo mappings to match observations. They include **Sub-Halo Abundance Matching (SHAM)** methods that establish a monotonic relationship between a galaxy property, such as stellar mass or luminosity, and a property of its host

dark matter halo, like its mass or peak velocity (the fundamental premise is that the most massive galaxy resides in the most massive halo) (Conroy et al. 2006; Moster et al. 2010; Dubois et al. 2014c; Tacchella et al. 2013; Moster et al. 2013, 2018; Tacchella et al. 2018); and **Halo Occupation Distribution (HOD)** methods, which specify the probability distribution for a halo of a given mass to host a certain number of galaxies (Peacock & Smith 2000; Berlind & Weinberg 2002a; Zheng et al. 2005; Guo et al. 2015; Rodriguez et al. 2015). While the physical-driven methods are more precise, they are computationally expensive and not the primary choice for LSS studies.

From the empirical-based category, even if simplistic, they have proven remarkably successful in reproducing a wide range of galaxy statistics, including clustering and lensing (Hearin et al. 2014), with several key contributions over the last years. A major lesson from these studies, however, is that, while halo mass can be the leading property that links galaxies with halos (White & Rees 1978), it cannot always by itself explain the observed clustering, especially on small scales (Yuan et al. 2021, 2022; Wu et al. 2024; Hadzhiyska et al. 2020; Paviot et al. 2024).

Halo occupation by galaxies can also depend on secondary halo properties, including assembly history—with earlier forming halos more clustered (Sheth & Tormen 2004; Gao et al. 2005; Wechsler et al. 2006; Han et al. 2019a; Dalal et al. 2008; Angulo et al. 2008; Li et al. 2008; Faltenbacher & White 2010; Lazeyras et al. 2017; Salcedo et al. 2018; Han et al. 2019b; Sato-Polito et al. 2019; Ramakrishnan et al. 2019; Tucci et al. 2021; Montero-Dorta et al. 2021; Balaguera-Antolínez et al. 2024)—, structural properties such as concentration and spin (Han et al. 2019a; Faltenbacher & White 2010; Sato-Polito et al. 2019; Montero-Dorta et al. 2021), and environmental factors (Kauffmann et al. 2004; Hahn et al. 2007; Blanton et al. 2006; Abbas & Sheth 2007; Wu et al. 2024; Pujol et al. 2017; Paranjape et al. 2018; Balaguera-Antolínez et al. 2024). For a review of this topic, we refer the reader to Wechsler & Tinker (2018).

Galaxies inherit the secondary bias of their host halos, which influences the baryonic processes they undergo and, consequently, their growth and evolution. The strength of this inheritance depends on the galaxy type. Luminous Red Galaxies (LRGs) which quenched their star formation early, are primarily shaped by their halos' assembly history rather than their current mass, making secondary halo bias a key driver of their properties. In contrast, Emission-Line Galaxies (ELGs) are actively forming stars, relying on the gas currently available in their halos, which is primarily determined by the halo's present mass. As a result, ELGs are largely insensitive to secondary halo biases. However, we note that ELGs exhibit clear environmental preferences, favoring lower-density regions such as filaments and sheets (Gonzalez-Perez et al. 2020). Thus, while a mass-based approach may captures their overall clustering, incorporating these environmental intricacies becomes important for high-precision analyses or studies of small-scale galaxy evolution (Favole et al. 2016; Gonzalez-Perez et al. 2020; Hadzhiyska et al. 2020; Rocher et al. 2023; Yu et al. 2024; Yuan et al. 2025).

The subtle dependencies that define the galaxy–halo connection also affect void physics, since voids are traced indirectly through galaxies. Several studies have explored this interplay from different perspectives. HOD-based analyses and observations have shown that voids host distinct galaxy populations—fainter, bluer, and younger galaxies residing in halos with fewer satellites (Blanton & Moustakas 2009a; Alfaro et al. 2022; Domínguez-Gómez et al. 2023; Conrado et al. 2024)—and that void statistics are sensitive to variations in HOD parametrizations, including environmental effects in galaxy formation (Ben-

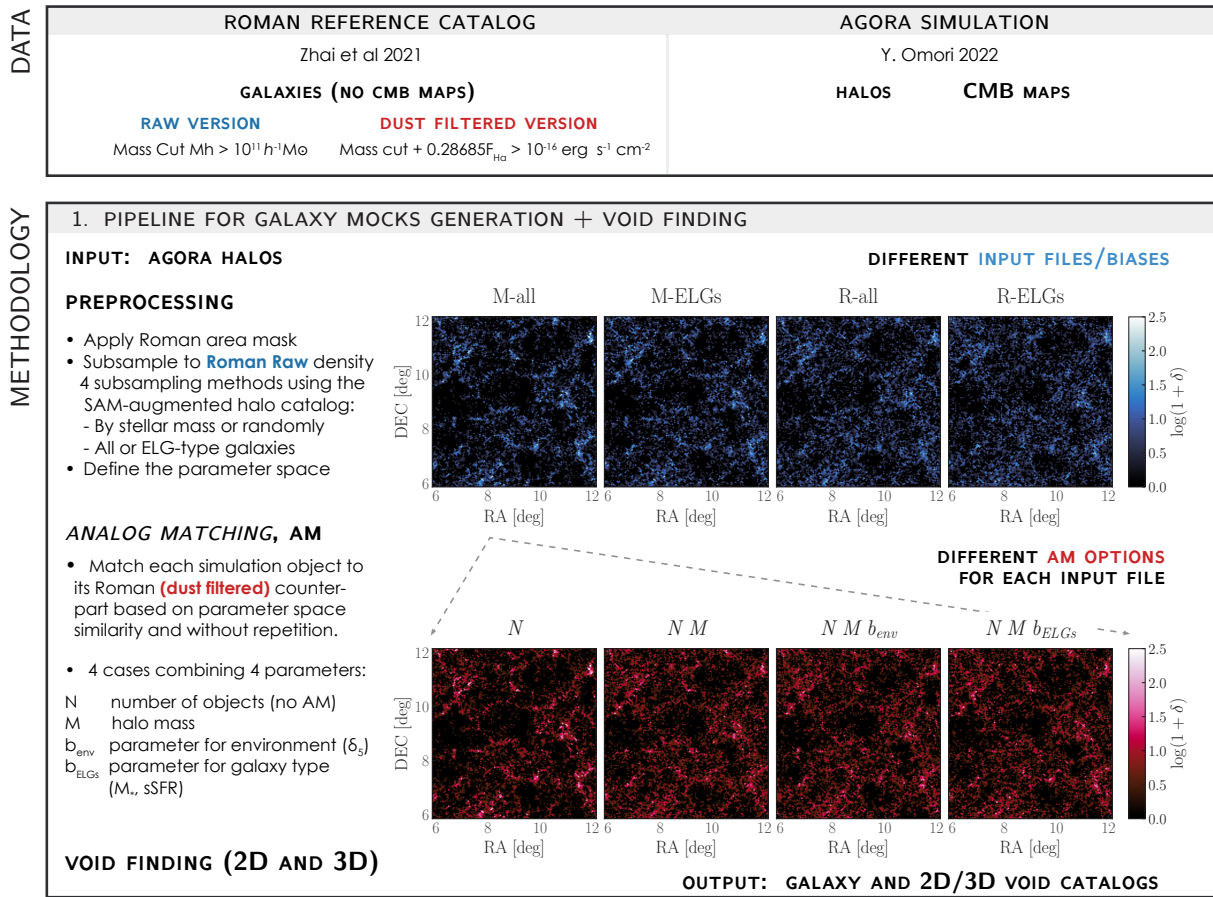


Fig. 1: Flowchart illustrating the datasets and methodology employed in this paper.

son 2001; Tinker et al. 2006a). The work of Nadathur & Hotchkiss (2015a) demonstrated that using unbiased dark matter particles as tracers—subsampled to match the mean galaxy number density, as was common in early analyses—fails to capture the effects of galaxy bias, leading to significant discrepancies in void counts and density profiles. At fixed sampling density, biased tracers produce far fewer small and intermediate voids, with differences comparable to those induced by changes in cosmological parameters.

Simulations have revealed that halo secondary properties, such as spin and concentration, also differ in voids: low-mass halos tend to have lower spin, more elongated shapes, and are more dynamically relaxed due to reduced merger activity, while mass-related quantities (like halo mass or peak velocity) remain largely unchanged (Balaguera-Antolínez et al. 2024).

Furthermore, there are studies that have assessed the extent to which galaxy voids trace the underlying dark matter field (Sutter et al. 2014a). Yet, no previous work has systematically investigated how different mock catalogs and modeling complexities impact both void statistics and the Void \times CMB correlation studies.

3.2. Our method: analog matching

In this work, we do not need to construct a mock catalog from scratch to match an observational dataset. We instead rely on the *Roman* mock catalog by Zhai et al. (2021) as a reference. Since this catalog does not include any CMB-related observable, our aim is to generate an analogous simulation that does provide

such synthetic CMB data, like the AGORA simulation. The overall workflow of our methodology is summarized in Fig. 1.

Our approach towards creating the mock catalog, which we call *analog matching*, does not fall into the aforementioned standard physical or empirical categories, although it shares some of their principles. The core of the procedure is to identify an AGORA halo counterpart for each *Roman* mock galaxy using a nearest-neighbor search implemented with the Python package KDTree (Virtanen et al. 2020). A KDTree is a non-parametric data structure optimized for nearest-neighbor searches in k -dimensional spaces that can capture complex, non-monotonic correlations beyond simple rank-order models. Nearest-neighbor methods are common analytical tools in cosmology — for example, to extract higher-order statistics of the density field (Banerjee & Abel 2021) — but have also been applied in mock catalog generation (Hearin et al. 2020; Wechsler et al. 2022).

Initially, the *Roman* reference mock catalog contains more than ten times the number of galaxies expected to be observed in the redshift range $1 < z < 2$. To reproduce realistic survey conditions, we adopt the Calzetti et al. (2000) dust model to scale the H α fluxes to the observed values and apply a flux cut to select only detectable galaxies. The resulting working dataset includes: a raw galaxy catalog, containing all sources⁹ and a dust-filtered catalog, which represents the realistic observed sample after the flux cut is applied. In both cases we impose the halo mass threshold of $10^{11} h^{-1} M_\odot$, to match the resolution of the AGORA simula-

⁹ satisfying: $\max(\text{H}\alpha, [\text{O III}]) > 5 \times 10^{-18} \text{ erg s}^{-1} \text{ cm}^{-2}$ (dust-free flux) and $H < 25$ assuming dust attenuation with $A_V = 1.6523$.

tion, leading to negligible changes (1.32%) in the dN/dz for the dust-filtered catalog and the redshift range considered.

Each *Roman* galaxy is represented in a multidimensional parameter space by a vector, $\chi_{i,\text{REF}}$, whose components include halo mass, environmental indicators, and other galaxy properties such as stellar mass or specific star formation rate. An equivalent vector, $\chi_{i,\text{AGORA}}$, is computed for the AGORA halos and a KDTree is used to establish a correspondence between both.

An important consideration is that finding counterparts between two samples can produce duplicates; that is, a single AGORA halo could be the closest match for multiple *Roman* galaxies. To prevent this, once a halo has been assigned, it is removed from the pool of available neighbors. Consequently, the order of the pairing is important. Since the first objects to be matched receive the closest neighbors and are therefore represented most faithfully, a criteria for the matching order is needed. Following the logic of abundance matching, we prioritize halos by mass, assigning them first, since mass is the main driver of clustering. This guarantees that most massive halos are accurately represented in the new catalog.

a) Halo catalog preprocessing: Parameter Computation and Subsampling.

To extend the parameter space beyond halo mass, we couple the **MULTIDARK PLANCK 2** halos embedded in AGORA to the **UNIVERSE MACHINE** galaxy formation model (Behroozi et al. 2019), which predicts stellar mass (M_*) and star formation rate (SFR) for each subhalo. From these, we assign stellar mass and the specific star formation rate $\text{sSFR} = \text{SFR}/M_*$ to each halo in AGORA, and use the bimodal sSFR distribution in the M_* –sSFR plane (Blanton & Moustakas 2009b) to distinguish between star-forming galaxies (including ELGs) and quenched galaxies (including LRGs), following the same approach as **Skyline** (Sato-Polito et al. 2023b). We then mask the AGORA simulation to match the *Roman* survey footprint and subsample it to the expected *Roman* galaxy number density, so that the number of AGORA parent halos (subhalos) equals the number of central (satellite) galaxies in the *Roman* mock catalog.

Using the aforementioned baryonic properties mapped to AGORA halos we perform the subsampling in four ways: ranking halos by their assigned stellar mass or choosing them randomly, and in each case selecting either all-type galaxies or only ELGs (see Figure B.1). The subsampling serves several purposes. First, by reducing the number of halos, it creates more manageable files which speed up the performance of KDTree. Second, it ensures a fair comparison between the *Roman* reference catalog, which contains only galaxies, and AGORA, which contains halos. Subsampling allows us to select a subset of halos that could correspond to potential observed galaxies. Later on, with the *analog matching* algorithm, we would further bias this selection towards something that resembles the dust-filtered *Roman* mock catalog. We consider, however, that this step poses a more realistic baseline to compare with. Third, explore how different subsampling strategies or tracer selections in the AGORA simulation affect the performance and robustness of the analog-matching algorithm.

To complete the parameter set, we account for environmental effects by computing the mass-weighted density contrast, formally defined as follows:

$$\delta_R^{(i)} = \frac{\sum_i M_h}{\langle M_h \rangle} - 1 \quad (4)$$

where, for each tracer, we count the number of neighboring tracers within a sphere of radius \mathcal{R} , weighting them by their halo masses and normalizing by the mean halo mass in the corresponding redshift bin and inside the same volume. We choose $\mathcal{R} = 5 h^{-1} \text{ Mpc}$ following previous studies (Balaguera-Antolínez et al. 2024; Wu et al. 2024) that claim that this radius effectively captures small-scale clustering.

We weight by halo mass, M_h , to emphasize the different environments in which galaxies can live. Although the *Roman* catalog is flux- and magnitude-limited, its raw version is denser than the dust-filtered sample and therefore provides a better approximation of the underlying matter distribution. To enable a consistent comparison, we compute the density contrast in the raw catalog and in the sub-sampled AGORA files (for each of the four different biases). These calculations are performed for each central galaxy, after which satellites are assigned the density contrast of their central (or closest central).

We need to take into account that the *analog matching* algorithm is applied to the final, dust-filtered catalog rather than the raw one even though some properties such as the environmental parameter (δ_R) is computed from the raw sample. We use the dust-filtered version to ensure that the best-fitting analogs from the sub-sampled AGORA simulation are reserved for the galaxies that will actually comprise our final sample. By doing this, we avoid wasting close neighbors on galaxies that would later be discarded by observational cuts.

b) Analog Matching through KDTree.

After defining the parameter space, χ , for both the sub-sampled AGORA simulation and the *Roman* dust-filtered reference catalog, we standardize each parameter to ensure that all the properties contribute equally to the matching. For each AGORA halo attribute $\chi_{i,\text{AGORA}}$, (halo mass, environment parameters, stellar mass, specific star formation rate), we subtract the mean of the corresponding parameter in the *Roman* catalog and divide by its standard deviation:

$$\chi_{i,\text{AGORA,STAND}} = \frac{\chi_{i,\text{AGORA}} - \bar{\chi}_{i,\text{REF}}}{\sigma_{\chi_{i,\text{REF}}}}. \quad (5)$$

Standardizing with respect to the *Roman* catalog ensures that the matching is properly weighted toward the observed sample. We then rank halos by mass, from most to least massive, and assign nearest neighbors in the standardized parameter space. If a halo has already been matched, the algorithm selects the next-closest available neighbor, ensuring a one-to-one correspondence while prioritizing the most massive, and thus most clustering-relevant, halos.

On this basis, we construct four families of mock catalogs, each reflecting a different level of specification. The names of the four mock catalogs are:

- *N* (number): This serves as a baseline method and no *analog matching* is applied at this stage. The procedure is the same as the first subsampling of the AGORA files (with four different biases), but in this case we directly match the number density of the dust-filtered catalog, without considering detailed halo properties.
- *NM* (halo mass): This method uses the *analog matching* technique with halo mass alone.

NM_{env} (halo mass and environment measures): This approach accounts for both halo mass and the local environment, quantified by δ_5 .

- NM_{ELGs} (halo mass and galaxy-type indicators): This method integrates halo mass and a parameter indicative of galaxy type, such as the stellar mass (M_*) and the star formation rate (SFR). This is the most similar to a SAM approach.

Each catalog type is generated for the four initial AGORA subsampling variants using the baryonic information of the SAM-augmented halo catalog (by stellar mass or randomly, considering either all galaxy types or only ELGs) resulting in a total of sixteen mock catalogs: four mock types, each run for four slightly differently biased files (see Figures 1 for a schematic explanation and B.1 for clarification purposes).

c) Tests

We validate the resulting catalogs by comparing them to the dust-filtered catalog across a number of one-point and two-point statistics. The former group includes galaxy and void redshift distributions, void size functions, and void minimum density distributions, while the latter includes the matter power spectrum and the void–galaxy cross-correlation function.

Strengths and limitations

While our methodology is not designed to compete with the most sophisticated empirical frameworks for mock catalog generation (our aim is to simply create analog catalogs from already existent ones), it represents a relevant middle ground. By incorporating multiple galaxy and halo properties simultaneously, it captures complex, multivariate relationships that one-dimensional methods such as SHAMs cannot resolve. At the same time, the use of KDTrees ensures that even large datasets can be processed efficiently, enabling fast generation of diverse mock realizations.

Naturally, the method carries certain limitations that must be acknowledged and which we address and discuss next.

- Parameter consistency: One potential issue appears when physical properties are defined or computed differently across datasets. Some features, such as the local environment, intended as a proxy for the matter distribution surrounding each galaxy, are affected by sample biases. In the reference mock, even by using the raw catalog which includes more galaxies than the dust-filtered version, the sample is still biased due to selection cuts. To make a fair comparison, we subsample the AGORA halo catalogs to the number density of the raw mock catalog, exploring multiple subsampling strategies to emulate these biases. If that is still different, comparisons of the corresponding parameters can lead to inconsistent pairings and systematic deviations in one- and two-point statistics.
- Spatial completeness and masking: Observational systematics that affect the spatial distribution of the observed galaxies, such as survey edges or other completeness losses, are not included in the algorithm, as these are absent in the reference catalog. In our method, these effects must be applied as a pre-processing step on the initial AGORA halo files. Since the *analog matching* is designed to fix the number density by finding, uniformly across the footprint, a counterpart for every reference object, applying completeness variations is

necessary beforehand, to preserve the desired number density while reproducing the spatial variations. If applied afterwards, objects would need to be removed to match the completeness, thereby reducing the desired number density.

- Ranking order: Finally, enforcing unique matches (so that each simulated object is assigned to only one reference object) means that the order of assignments can affect results, potentially leading to suboptimal pairings in crowded regions of parameter space. Although alternative strategies could be explored, we prioritize a mass-based ranking inspired by SHAM methods, which has proven effective for our purposes.

3.3. Cosmic voids as mock validation tools

To further probe the galaxy distribution beyond 2-point correlation functions, we analyze the statistical properties of cosmic voids in our mock catalogs. From a theoretical perspective, voids (and halos) were traditionally modeled using a combination of the excursion set formalism and the spherical collapse model (Sheth & van de Weygaert 2004b; Jennings et al. 2013b). In this mathematical framework, the statistical distribution of structures is modeled by representing the primordial density field as an ensemble of random walks, which trace how the local density contrast, δ , at a fixed position changes when we vary the smoothing scale, R . At large smoothing scales, fluctuations are averaged over wide regions and the density field appears nearly uniform. But as R decreases, the filter begins to include more local fluctuations, making δ wander upward or downward like a random path.

A structure is said to form at the characteristic scale R where this random walk first crosses a critical threshold value, known as the "barrier". For halos, this barrier is a fixed positive overdensity threshold (δ_c), physically anchored to the events of gravitational collapse and virialization. For voids, it is a negative barrier (δ_v) which has a different meaning. Voids evolve fundamentally differently: they simply grow faster than the background and continue their outward expansion forever without experiencing a characteristic formation event. In the past, the value of shell-crossing—when a void's inner shells expand and overtake its outer shells—was proposed to mark formation, but recent work demonstrates that this event is likely unphysical for realistic profiles and occurs at depths that galaxy surveys cannot trace. Consequently, the value for the void threshold (δ_v) is flexible as long as it is kept consistent in the theoretical set-up and the observational counterpart measured in surveys (Verza et al. 2024a).

In practical terms, the definition of a void is less clear. When dealing with simulations or survey data, an algorithmic approach is needed and a number of different void finders have emerged (see Colberg et al. 2008; Cautun et al. 2018; Paillas et al. 2019, for a review of methods). Lavaux & Wandelt (2010) group these algorithms into three categories: density-based, which identify underdense regions using smoothed density fields and often assume spherical shaped voids (Sánchez et al. 2017; Paz et al. 2023); geometrical-based finders, which use tessellation techniques to rely on the topology of the density field and do not make assumptions about void geometries (Platen et al. 2007; Neyrinck 2008); and dynamical-based, which rely on the dynamics of the matter distribution through the displacement or velocity fields (Lavaux & Wandelt 2010).

Studies are actively working to bridge the gap between the theoretical and the observational definition (Nadathur &

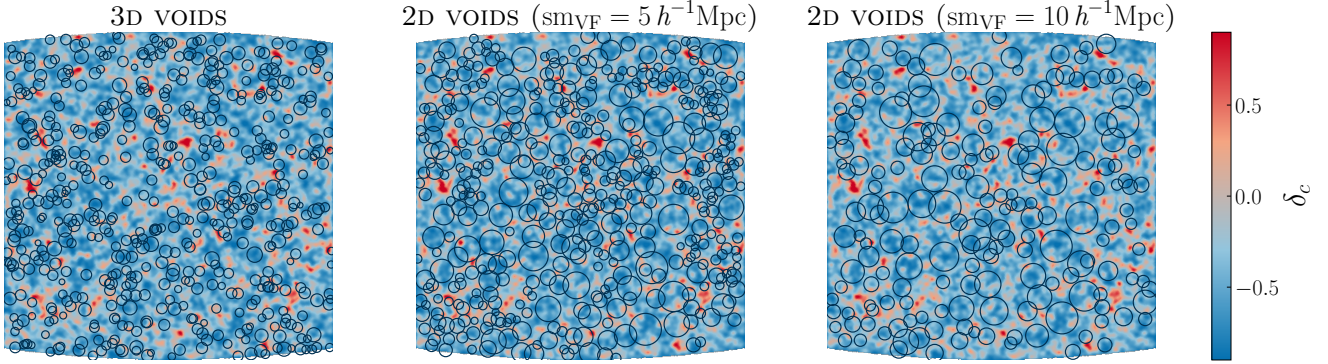


Fig. 2: Slice at $z = 1.012$ with thickness $\Delta z = 0.01$, illustrating 3D and 2D voids identified with the void finder with smoothing scales of 5 and $10 \text{ Mpc } h^{-1}$. To maintain clarity, only voids centered at this exact redshift are plotted; otherwise, including the full slice width would result in 3D voids covering the map. Specifically, we identify 525 3D voids (restricted to this redshift), compared to 470 2D voids at $\text{sm}_{\text{VF}} = 5 \text{ Mpc } h^{-1}$ and 209 at $\text{sm}_{\text{VF}} = 10 \text{ Mpc } h^{-1}$. Their average sizes are $24.91, 50.38$, and $83.90 \text{ Mpc } h^{-1}$ (corresponding to angular sizes of $0.42, 0.84$, and 1.48 degrees), respectively.

Hotchkiss 2015b; Correa et al. 2021b; Contarini et al. 2024). For example for the void size function a cleaning process is applied to ensure that the void sample is aligned in agreement with the theoretical definition¹⁰, and the recent work by Verza et al. (2024a) who reformulates the theoretical framework by combining the excursion-set approach with peak theory and introducing an effective moving barrier. In this view, voids form not around random positions but around local minima of the density field and the effective barrier varies with the scale and encapsulates non-sphericity, environmental tidal effects, and the statistical properties of density minima to reproduce the multiplicity function and void size function observed in simulations.

Given the zoo of available methods, one may wonder which is the best criteria to follow when choosing one. A pragmatic choice is to use the definition that allows us to extract the greatest signal from void samples in a given research context. For instance, 2D voids, where the projected voids lead to tunnels or troughs, are better suited for lensing observables (see e.g., Cautun et al. 2018). Advances on applying 3D void finders to photometric redshift data have however demonstrated their ability to identify orders of magnitude more voids and therefore to allow also precise lensing measurements (see Fang et al. 2019, for details).

This study does not aim to test any theoretical definitions but to simply quantify the impact of different mock catalogs on void statistics. For this, we employ both a 2D (density-based) and a 3D (geometrical) void finder since they are widely adopted and particularly relevant for forthcoming investigations of void \times CMB correlations.

2D Voids For identifying the 2D voids we make use of the algorithm by Sánchez et al. (2017). The code works by projecting galaxies into 2D slices and finding voids in the smoothed 2D galaxy density field of the slice. The void finding process involves the following steps:

(i) Divide the tracer sample into redshift slices of thickness s in co-moving distance. (ii) For each slice, a density contrast map is calculated by projecting tracers onto a HEALpix map¹¹

and smoothing the field with a Gaussian filter of co-moving scale sm_{VF} . (iii) Voids are identified by locating the most underdense pixels ($\delta < -\sigma_{\delta_c}$, ¹²) as initial centers, and a circular region of radius R_v is grown around each center until the mean density is reached. (iv) Identified void pixels are excluded from further consideration, and the process iterates until all pixels are assigned to voids. (v) Voids that extend beyond the survey boundaries by more than a defined fraction of their area are excluded. This is determined using a random point catalog by comparing the number of random points within each void to the expected count from the mean random-point density; those retaining less than a threshold fraction (e.g., 70 %) are deemed incomplete and removed. (vi) Finally to improve line-of-sight positioning, the slicing process is repeated with shifted centers, and voids in neighboring slices with small angular separations are grouped into single structures. The 3D positions of these grouped voids are computed as the median positions of their constituent members.

The 2D void identification depends on several free parameters, which influence the resulting void catalogs and observables (see e.g., Vielzeuf et al. 2021a). These include the Gaussian smoothing scale (sm_{VF}) applied to the projected galaxy density field, and the tomographic slice thickness, typically aligned with the photometric redshift scatter to ensure the detection of independent underdense structures (which is not applicable to our case). We adopt a smoothing parameter of $\text{sm}_{\text{VF}} = 10 \text{ Mpc } h^{-1}$ and a slice thickness of $s \approx 70 \text{ Mpc } h^{-1}$ although other configurations were tested¹³.

The outputs of the void finder are the position of the voids (ra, dec, z_{obs}); the transversal and radial sizes; the mean density contrast $\bar{\delta}(r < r_v) = \rho/\bar{\rho} - 1$ where ρ is the average density inside the void and $\bar{\rho}$ is the mean density of the corresponding redshift slice; and the central density contrast which corresponds to the density contrast evaluated at one quarter of the void radius $\delta_{1/4} \equiv \delta(r = 0.25 r_v)$.

¹⁰ The cleaning involves applying a density contrast threshold, removing intersecting voids, and rescaling remaining voids.

¹¹ $N_{\text{side}} = 512$ representing an angular resolution of 0.1 deg. and a physical resolution of $4 \text{ Mpc } h^{-1}$ at $z = 1$ ($6 \text{ Mpc } h^{-1}$ at $z = 2$).

¹² meaning the local density is lower than the cosmic mean by more than one standard deviation of the density fluctuations

¹³ Considering that we work with spec-zs, in contrast with e.g. Sánchez et al. (2017) who select thickness of $\sim 100 \text{ Mpc } h^{-1}$, that is related to the typical photo-z errors of LRGs they worked with.

3D Voids For identifying 3D voids, we used REVOLVER¹⁴ (REal-space VOid Locations from surVEy Reconstruction) void-finding code, based on a modified version of the ZOBOV algorithm (Neyrinck 2008). The void identification process includes the following steps: (i) The tracer density field is reconstructed using a Voronoi Tessellation Field Estimator (VTFE), which divides the survey volume into Voronoi cells—one per tracer—and assigns each cell a density equal to the inverse of its volume. (ii) Void centers are identified at local minima, and neighboring regions are merged by following rising density gradients to form contiguous “zones”. Boundaries between voids are identified at saddle points, i.e., where the density stops increasing and begins to slope toward an adjacent minimum. These ridges delineate distinct density basins, each of which is treated as an independent void without further merging. (iii) Void centers are assigned as the circumcenter of the lowest-density tracer and its three lowest-density adjacent neighbors (although the volume-weighted barycenter is also provided for comparison purposes)¹⁵ (v) Finally, the effective void radius is determined as the radius of a sphere with a volume equal to the total volume of the constituent Voronoi cells.

Tracers on the edge of the mask could have arbitrarily large Voronoi volumes since they are not surrounded by anything else. To take into account the effect of the mask, the code overflows this forbidden regions with mock tracers, simulating overdense section of space. Density estimates associated with these buffer particles and any tracers adjacent to them are identified and removed before the watershed stage.

The output of REVOLVER includes: the void ID; the void center (\mathbf{X}_v) with both the circumcenter and barycenter; the effective spherical radius (R_v); the central density contrast ($\delta_{v,\min}$); the average density contrast ($\bar{\delta}_v$); the density ratio, i.e., the ratio of the highest density at the void’s edge to the minimum density at the center; and the dimensionless parameter (λ_v), a proxy for the gravitational potential, which distinguishes different void populations and plays a role in their lensing properties (see e.g. Sheth & van de Weygaert 2004a; Raghunathan et al. 2020). Negative λ_v indicates large underdense voids (void-in-voids), while positive values correspond to smaller overdense regions (void-in-clouds):

$$\lambda_v \equiv \bar{\delta}_v \left(\frac{R_v}{1 h^{-1} \text{Mpc}} \right)^{1.2}. \quad (6)$$

ZOBOV operates with minimal assumptions and no free parameters which allows to topologically detect voids purely from the density field.

4. Results

In this section, we present and discuss the results, with a focus on the impact of mock catalog variations on the resulting galaxy clustering and void statistics.

4.1. One-point statistics

For galaxies, the one-point statistics essentially corresponds to the number density. We ensure that this matches the reference

¹⁴ <https://github.com/seshnadathur/Revolver>

¹⁵ The circumcenter is the point equidistant from all chosen vertices, representing the geometric center of the underdense region, while the barycenter is the arithmetic mean of all points weighted by their cell volume.

mock catalog by construction, since each galaxy is assigned a corresponding analog in the AGORA simulation. For voids, the one-point statistics we analyze are: void redshift distribution, void size function, and minimum density distributions.

All plots in the paper follow a consistent layout to maintain clarity. Each column corresponds to a different type of mock catalog: the first column shows the catalog produced by subsampling (N), to match the number density per redshift bin of the reference catalog; the second columns shows the mock catalog generated using the *analog matching* method based on halo mass alone (NM); the third applies the same method but incorporates both halo mass and environment (NM_{env}); and the fourth includes halo mass and two parameters (stellar mass and SFR) that encode information about the galaxy type (NM_{ELGs}). Each subplot displays the residuals of the corresponding observable relative to the reference case.

Within each of the above methods (and thus in each column), we show four variants that reflect different tracer biases. As explained in the methodology, before applying the *analog matching* procedure, we subsample our simulation files in four different ways to match the number density of the raw *Roman* galaxy catalog. This makes the files more manageable for computing the KDTree, and allows us to see how the tracer biases in the input files affect the *analog matching* performance.

The four variants are random subsampling (R) or by stellar mass (M), and selecting either all galaxies (-all) or only ELGs (-ELGs). For the first mock catalog type (N), we directly subsample to match the number density of the dust-filtered catalog (i.e. not the raw catalog) using the four subsampling criteria (R-all, R-ELGs, M-all, M-ELGs).

Figure 3 shows the one-point statistics for 2D and 3D voids. The largest discrepancies with respect to the reference case are observed for the N and NM_{env} mock catalogs. For the subsampling catalog (N), the mass-selected sample shows the biggest deviation. This is expected, as the ELGs more typically inhabit lower-density regions and selecting the most massive tracers emphasizes clusters and filaments in the cosmic web, resulting in fewer voids which are larger and deeper.

When selecting tracers by both stellar mass and ELG-type, the distribution becomes closer to the reference case. Mock galaxies are now present in lower-density regions as well, which increases the number of voids, as the previously-large voids are subdivided into smaller ones. Randomly selecting tracers further amplifies this effect, creating even more fragmented and shallower voids since tracers populate all types of environments in this case. These random-selected samples, either for the case of all galaxy types or only ELGs, are very similar. Overall, none of the N -type mock catalog selections fully reproduce the trend observed in the reference catalog, although the R-ELG and R-all cases show comparatively good agreement.

For the NM_{env} catalog, in the third column of each block of plots, the observed discrepancies stem from the algorithm itself, highlighting one of the aforementioned limitations of the *analog matching* method. This technique requires that the quantities compared between the reference mock and the target simulation represent the same physical property. The b_{env} parameter, which quantifies the environment through the density contrast in spheres of $5 h^{-1}$ Mpc, is heavily influenced by the type of tracer used. Ideally, we would compute b_{env} directly from the dark matter field for both datasets, but as mentioned, the raw mock galaxy catalog includes only objects with no information about the full halo population or the underlying matter field. Among the subsampled AGORA halos, designed to replicate the bias of the ref-

1 POINT STATISTICS

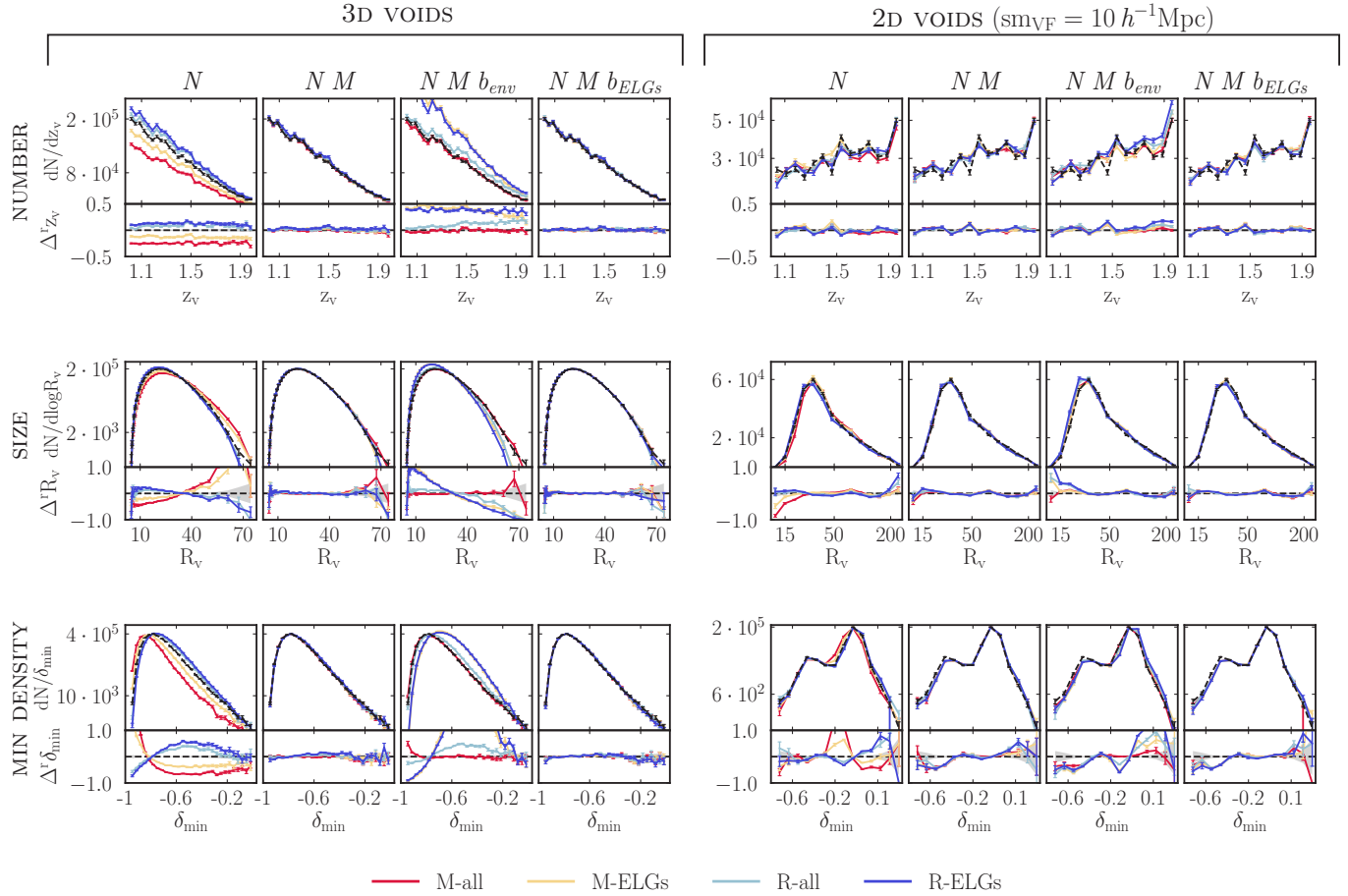


Fig. 3: One-point statistic distributions for the generated void catalogs. The rows correspond to the void redshift (top), void size (middle), and minimum density (bottom) distributions for the respective void samples. Each column represents a different mock catalog type. Different colors denote a different tracer bias. The bottom sub-panels display the residuals, defined as the relative difference with respect to the *Roman* reference catalog. Error bars are Poissonian.

ference mock catalog, the mass-selected sample reproduces its properties most closely (see Appendix B.1 for details).

For the *analog matching* cases based on halo number and mass (*NM*), or the more complex implementation including mass and b_{elg} (NMb_{elg}), we find excellent agreement with respect to the reference case. Neither of the two options shows a clear advantage, suggesting that halo mass alone is sufficient to reproduce void statistics coming from ELGs. The largest deviations occur only at the extreme values of δ_{\min} , for very large or very shallow voids, but the overall trends remain consistent.

All the effects discussed can be seen more clearly for 3D voids. 2D voids under the standard smoothing scale of $10 h^{-1}$ Mpc wash out much of the catalog-to-catalog variation. If we reduce the smoothing to $5 h^{-1}$ Mpc, the differences start to be apparent although still more subtle than for the 3D case (see Appendix Fig. C.1).

4.2. Two-point statistics methods

We extend our analysis to two-point statistics by examining the galaxy angular power spectrum and the void-galaxy cross-correlation function for both 2D and 3D voids. We first de-

fine these quantities, describe how they are computed, and then present and discuss the results.

The **angular power spectrum**, C_ℓ , quantifies the clustering of matter, in 2D projected count maps, by measuring the variance of density fluctuations as a function of angular scale $\ell \sim \pi/\theta$. Higher C_ℓ amplitudes point to stronger anisotropies, corresponding to either overdense regions (clusters) and/or underdense regions (voids). Lower amplitudes indicate relatively uniform regions with little structure. We compute the C_ℓ s using NaMaster (Alonso et al. 2019), and the error bars are estimated from the standard expression (Knox 1995):

$$\sigma_{C_\ell} = \sqrt{\frac{2}{(2\ell+1)f_{\text{sky}}}} (C_\ell + N_\ell), \quad (7)$$

where f_{sky} is the observed sky fraction, C_ℓ the angular power spectrum, and N_ℓ is the shot noise power spectrum, equal to $N_\ell = 1/\bar{n}_g$, with \bar{n}_g the average galaxy angular number density.

The **Void-Galaxy Cross-Correlation Function** (VGCF), $\xi(r, \mu)$, measures the excess probability of finding a galaxy at distance r (from a void center) and angle $\mu = \cos \theta$ (with respect to the line-of-sight pointing to the void center), compared

2 POINT STATISTICS

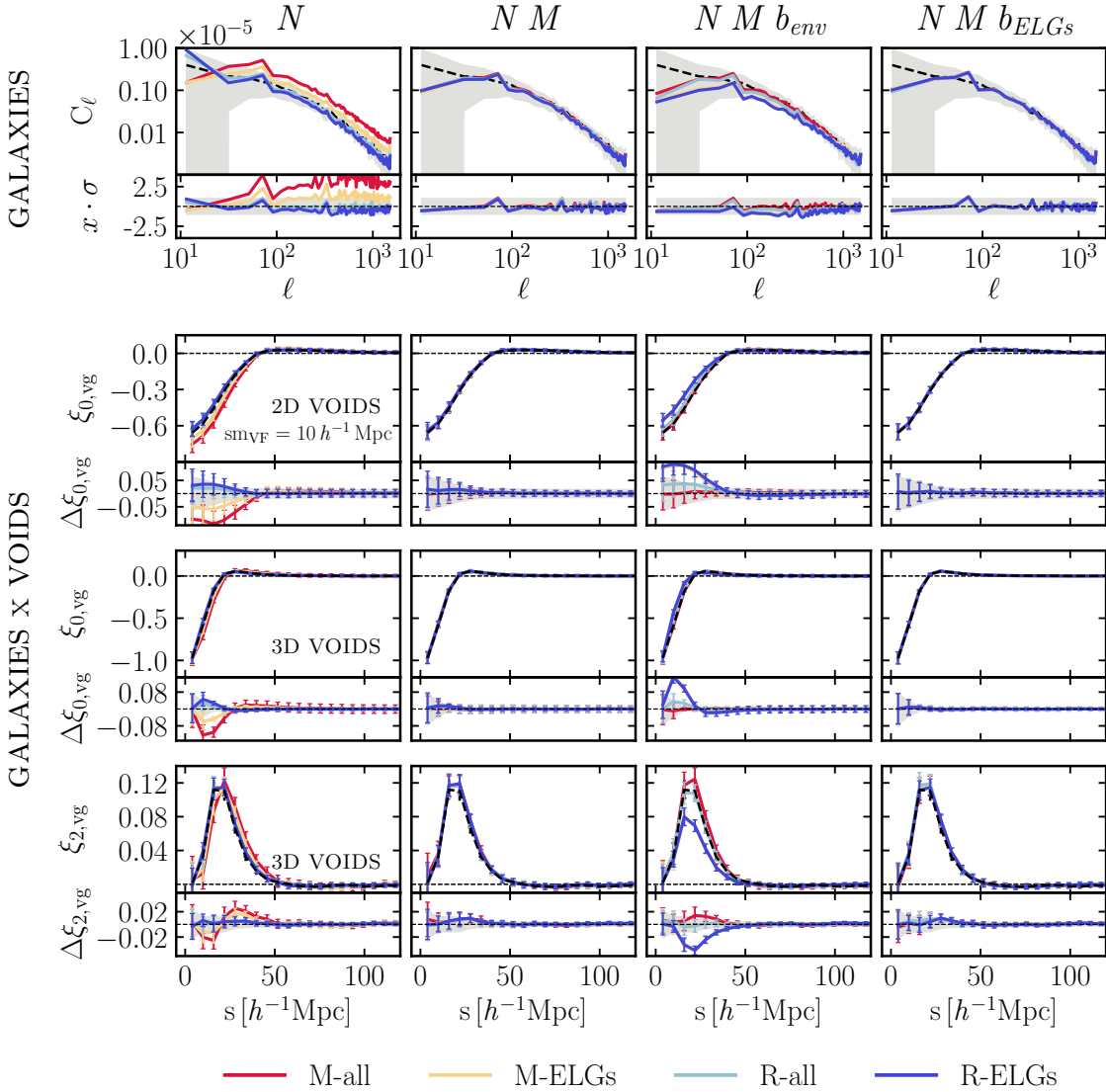


Fig. 4: Two-point statistics including the galaxy power spectrum (top panel) and the galaxy-void cross-correlation function. For the latter, the monopole of both 2D and 3D voids and the quadrupole of the 3D voids are included. Each column corresponds to a different mock catalog type, and each color represents a different tracer bias. The residuals in the bottom sub-panels show the relative difference compared to the *Roman* reference catalog. Error bars are derived from jackknife estimates.

to a random and unclustered galaxy distribution. Under the cosmological principle, which states that the Universe is statistically homogeneous and isotropic on large scales, stacked voids should appear spherical when averaged implying that $\xi(r, \mu)$ would depend only on r (Lavaux & Wandelt 2012). However, the observed VGCF reveal anisotropies due to two effects: dynamical distortions from galaxy peculiar velocities along the line of sight (redshift-space distortions, RSD), and geometrical distortions from adopting an incorrect cosmological model when converting redshifts and angles into distances (Alcock–Paczynski effect, AP, Alcock & Paczynski 1979). By modeling these distortions, the VGCF has become one of the standard tools in void cosmology for constraining cosmological parameters (Alcock & Paczynski 1979; Ryden 1995; Sutter et al. 2012; Mao et al. 2017; Nadathur et al. 2020; Hamaus et al. 2020, 2022; Woodfinden et al. 2022; Correa et al. 2022a; Radinović et al. 2023; Verza

et al. 2024b; Fraser et al. 2025; Degni et al. 2025). We measure the VGCF using the Landy–Szalay estimator (Landy & Szalay 1993):

$$\xi(r, \mu) = \frac{\langle D_v D_g \rangle - \langle D_v R_g \rangle - \langle R_v D_g \rangle + \langle R_v R_g \rangle}{\langle R_v R_g \rangle}, \quad (8)$$

where D and R refer to data and random catalogs, respectively, and angled brackets indicate normalized pair counts between void centers (v) and galaxies (g). The estimator works by comparing the observed void-galaxy pair counts to those from synthetic random catalogs of voids and galaxies that share the same survey volume and selection function but contain no intrinsic clustering. In this work, we compute pair counts in 25 equally spaced bins in both r and μ using `Corrfunc` from Sinha & Garrison (2020).

Once $\xi(r, \mu)$ is computed, we separate isotropic and anisotropic contributions by expanding it into multipoles with Legendre polynomials $P_\ell(\mu)$:

$$\xi_\ell(r) = \frac{2\ell+1}{2} \int_{-1}^1 \xi(r, \mu) P_\ell(\mu) d\mu. \quad (9)$$

The **monopole**, $\xi_0(r)$, describes the average radial density profile of galaxies around voids. It is negative inside the void (fewer galaxies than average) and positive in the surrounding shell.

The **quadrupole**, $\xi_2(r)$, captures the anisotropic distortions induced by RSD and AP effects. A null quadrupole indicates spherical symmetry while a negative or positive signal reflect deviations from sphericity. In particular, a positive quadrupole reflects elongation along the line of sight, typically from galaxy outflows, whereas a negative quadrupole indicates infall and a prolate shape. In our case, the small negative bump observed in $\xi_2(r)$ in Figure 4, suggests the presence of compensation walls, where galaxies move inward from outside the void toward its edges.

Uncertainties are estimated via a jackknife resampling method. The galaxy and void samples are partitioned into $N = 70^{16}$ spatial regions using the k -means clustering algorithm (scikit-learn; Pedregosa et al. 2011). For each realization, one region is omitted, and the correlation function is recomputed with the remaining data. The covariance matrix is then computed as:

$$C_{ij} = \frac{N-1}{N} \sum_{k=1}^N [\xi^{(k)}(r_i) - \bar{\xi}(r_i)][\xi^{(k)}(r_j) - \bar{\xi}(r_j)], \quad (10)$$

where $\bar{\xi}(r)$ is the mean of the jackknife realizations. The diagonal elements of C_{ij} provide the variance and hence the error bars on the measurements.

When displaying the results, the plots are organized in the same way as for the one-point statistics. Every column represents one of the mock catalog types (N :number; NM : number and mass; NM_{env} : number, mass and environment; NM_{ELGs} : number, mass and type of galaxy). Within each column, colors distinguish different biases: M-all, M-ELGs (mass-selected), R-all, R-ELGs (random-selected).

4.3. Void-galaxy correlation results

The results of the two-point statistics are complementary to and consistent with the one-point statistics. The dispersion is larger for the N and NM_{env} cases, whereas NM and NM_{ELGs} show good agreement with the reference catalog. Galaxy clustering strength, measured by the angular power spectrum (C_ℓ), is directly related to the galaxy bias (b). This is clearly seen for the N mock type, in the first column, where the different tracer selections produce a clear progression from most to least clustered with respect to the *Roman* reference catalog. Mass-selected galaxies are the most clustered, and this leads to the strongest density fluctuations: high densities in knots and sheets and very low densities elsewhere.

In contrast, randomly selected galaxies are distributed more evenly throughout the cosmic web, leading to a more uniform

density field and weaker clustering. Selecting ELGs slightly reduce clustering in either case, smoothing out the overall density variations, as they preferentially occupy lower-density regions.

The monopole of the VGCF, $\xi_0(r)$, representing the average radial density profile, mirrors the same behavior as the C_ℓ clustering trends. The density is lowest for deeper voids of the M-all sample and becomes progressively shallower moving through M-ELGs, R-all, and R-ELGs. The zero-crossing point, which is linked to the average void radius, shows that voids are larger in mass-selected samples, in agreement with the trends observed in the one-point statistics. This progression highlights how galaxy bias influences void morphology: stronger clustering produces more pronounced density contrasts and larger voids, while weaker clustering leads to smoother profiles.

The quadrupole, $\xi_2(r)$, exhibits a similar amplitude across the different biased tracers but is shifted in radius, aligning with the average void size indicated by the monopole.

The NM_{env} method, as previously shown, only yields meaningful analogs when the galaxy bias in the mock catalog is similar to that of the reference catalog. If the bias differs, the same value of b_{env} can correspond to very different underlying environments, making the matching impossible. For instance, if the raw reference catalog is formed by a mass-selected sample of all type galaxies, as the results suggest, a low value of b_{env} may correspond to a void while for a random-selected sample, the same value of b_{env} could be found in a moderately dense filament, since the underlying dark matter distribution is sampled more uniformly in this latter case.

Still under the NM_{env} method, the ELG samples (either randomly or mass-selected) show a different behavior with respect the reference catalog, and a very similar behavior between them. Their effective bias seems to be lower than that of the reference catalog, the monopole is shallower for 2D and 3D voids, and the quadrupole is less distorted suggesting a less elongated void in redshift space.

Another important takeaway, that we can see in this mock type, is that similar galaxy clustering (i.e. similar C_ℓ power spectrum) does not guarantee similar void statistics. For example, the R-all sample have a power spectrum close to the M-all sample (and consequently to the reference case), but its voids differ significantly in size and density profile. This finding highlights that void statistics provide independent and sensitive information about how galaxies populate the cosmic web, beyond what is captured by the matter power spectrum which can be a powerful test for analyzing the accuracy of mock catalogs.

For the NM and NM_{ELGs} cases, all galaxy bias selections give consistent one- and two-point statistics, showing that the *analog matching* method can effectively remove the initial bias in AGORA files when the same physical parameters are matched for both AGORA and the reference catalog. The monopole and quadrupole are also very similar and fall within the error bars, making these the best match to the *Roman* reference catalog.

It is important to note that none of the methods perfectly reproduces the C_ℓ at low ℓ . This regime is dominated by cosmic variance, as reflected in the uncertainties. Cosmic variance arises because we observe only a single universe, and on very large scales there are few independent modes of density fluctuations to average over. This effect is further amplified when the survey does not cover the full sky, and measurements on these scales carry large statistical uncertainties.

We nevertheless consider that this lack of agreement at low ℓ is not a major concern for void studies since their key properties, such as the size distribution and density profiles, are primarily determined by smaller scales (higher multipoles). Our most ro-

¹⁶ We adopt this number to provide a sufficient number of jackknife realizations for a stable covariance estimate while maintaining regions large enough to capture the spatial correlations of voids and galaxies.

bust constraints are for scales below $\ell \sim 30$ ($\sim 5.7^\circ$), which corresponds to the largest 2D voids; with 3D voids being typically of smaller size.¹⁷

5. Discussion & Conclusions

The correlation between cosmic voids and the CMB—most notably the void×CMB lensing signal—has been firmly established observationally, with reported significances of $3\text{--}17\sigma$ (Cai et al. 2017; Chantavat et al. 2016; Raghunathan et al. 2020; Vielzeuf et al. 2021b; Hang et al. 2021; Kovács et al. 2022; Camacho-Ciurana et al. 2024; Demirbozan et al. 2024; Sartori et al. 2025). However, several studies have also identified moderate ($\lesssim 3\sigma$) tensions with respect to the ΛCDM predictions (Vielzeuf et al. 2021b; Hang et al. 2021; Kovács et al. 2022; Camacho-Ciurana et al. 2024), the origin of which remains unclear.

Properly interpreting these and future findings requires a careful distinction of methodological artifacts from genuine physical signals. Until the influence of analysis choices—such as void identification or mock catalog construction—is fully understood, observed tensions cannot be confidently attributed to physics beyond the standard cosmological model.

Motivated by this, and in preparation for the Nancy Grace *Roman* Space Telescope, we have developed an empirical framework designed to produce a set of *Roman*-like mock catalogs of varying degrees of fidelity ranging from basic dark matter subsamples—known to inadequately reproduce galaxy and void statistics (Nadathur & Hotchkiss 2015a)—to survey-specific realizations that accurately recover the clustering and bias properties of the *Roman* ELGs sample. These serve as a useful benchmark to investigate how catalog construction impacts different cosmological observables.

Our algorithm, called *analog matching*, reproduces existing galaxy mock catalogs in a simulation of interest. We employ the AGORA simulation since it provides a full-sky halo lightcone alongside coherently modeled CMB secondary anisotropy maps. Within this framework, each galaxy from the reference *Roman* mock catalog is associated with a halo in AGORA through a nearest-neighbor search in a flexible parameter space. This space is highly customizable and may be as comprehensive as the user desires, including—among other parameters—halo mass, environmental indicators, and, when available, galaxy properties such as stellar mass and sSFR mapped to halos via precomputed SAMs. Galaxies are processed in decreasing order of mass so that massive objects are paired with their most suitable analogs preserving the high-mass end of the distribution.

We validate the resulting mock catalogs by comparing their one- and two-point galaxy and void statistics against those of the reference *Roman* catalog:

- Our results confirm that both sets of statistics are highly sensitive to the details of the mock-construction process, consistent with previous studies (Berlind & Weinberg 2002b; Tinker et al. 2006b; Sutter et al. 2014b,c; Nadathur & Hotchkiss 2015a; Contarini et al. 2019b; Salcedo et al. 2025).
- Importantly, we find that matching based on halo mass alone (or halo mass and galaxy type) is sufficient to reproduce the clustering and void statistics of *Roman* ELGs, whereas

including environmental information can degrade the algorithm’s performance when the underlying dark matter field for both the simulation and the reference catalog is not available.

- Throughout this paper, we find that void statistics provide a powerful diagnostic for assessing mock catalog accuracy beyond traditional clustering measures, with 3D voids generally showing stronger dependence than 2D voids.

Looking ahead, it will be valuable to test how this methodology performs for tracers that exhibit stronger assembly bias, such as LRGs, for which halo mass alone is an insufficient predictor of clustering. Moreover, in forthcoming N-body simulations that include CMB companions and multiple cosmological realizations but lack baryonic information (e.g., M_* and sSFR), our method will require the reference catalogs to provide access to the underlying dark matter field. This will enable the computation of secondary halo bias indicators—such as tidal anisotropy, local matter density or cosmic-web classification (Balaguera-Antolínez et al. 2024)—to identify the halos where galaxies are most likely to be found, without assuming a direct link to galaxy bias.

In conclusion, rather than compete with the state-of-the-art mock-generation pipelines, our goal is to provide a validated suite of *Roman*-like mock catalogs of varying accuracy that can serve as a controlled testbed for void–CMB correlation studies and related analyses. In a companion paper, we use the data products generated here to assess the impact of mock catalog construction on the measured Void×CMB lensing signal.

Data availability

The main products from this work, including mock galaxy catalogues, void catalogues, and analysis codes, will be made publicly available after acceptance of the paper for publication. We are available for consultation about the results or our methodology.

Acknowledgements

This paper made use of the IAC HTCondor facility (<http://research.cs.wisc.edu/htcondor/>), partly financed by the Ministry of Economy and Competitiveness with FEDER funds, code IACA13-3E-2493. MP wishes to acknowledge the contribution of the IAC High-Performance Computing support team and hardware facilities to the results of this research, specially to Ángel de Vicente.

MP acknowledges support from the pre-doctoral program at the Center for Computational Astrophysics, Flatiron Institute. Research at the Flatiron Institute is supported by the Simons Foundation. MP acknowledges support from the Agencia Estatal de Investigación del Ministerio de Ciencia en Innovación (AEIMICIN) and the European Social Fund (ESF+) under grant PRE2021-098156. C.H.-M. acknowledges the support of the Spanish Ministry of Science and Innovation via project PID2021-126616NB-I00.

The Large-Scale Structure (LSS) research group at Konkoly Observatory has been supported by a *Lendület* excellence grant by the Hungarian Academy of Sciences (MTA). This project has received funding from the European Union’s Horizon Europe research and innovation programme under the Marie Skłodowska-Curie grant agreement number 101130774. Funding for this

¹⁷ 3D voids span $0.11^\circ\text{--}1.31^\circ$ ($4\text{--}81 h^{-1}$ Mpc, mean $22 h^{-1}$ Mpc) in the redshift range $1 < z < 2$. For 2D voids with $5 h^{-1}$ Mpc smoothing, sizes range $0.09^\circ\text{--}4.97^\circ$ ($5\text{--}264 h^{-1}$ Mpc, mean $33 h^{-1}$ Mpc), and with $10 h^{-1}$ Mpc smoothing, $0.19^\circ\text{--}5.93^\circ$ ($11\text{--}264 h^{-1}$ Mpc, mean $50 h^{-1}$ Mpc).

project was also available in part through the Hungarian National Research, Development and Innovation Office (NKFIH, grant OTKA NN147550).

AP acknowledges support from the European Research Council (ERC) under the European Union's Horizon programme (COSMOBEST ERC funded project, grant agreement 101078174), as well as support from the French government under the France 2030 investment plan, as part of the Initiative d'Excellence d'Aix-Marseille Université - A*MIDEX AMX-22-CEI-03.

References

Abbas, U., & Sheth, R. K. 2007, MNRAS, 378, 641, doi: [10.1111/j.1365-2966.2007.11806.x](https://doi.org/10.1111/j.1365-2966.2007.11806.x)

Abbott, T. M. C., Aguena, M., Alarcon, A., et al. 2023, Phys. Rev. D, 107, 023531, doi: [10.1103/PhysRevD.107.023531](https://doi.org/10.1103/PhysRevD.107.023531)

Abdalla, E., Abellán, G. F., Aboubrahim, A., et al. 2022, Journal of High Energy Astrophysics, 34, 49, doi: [10.1016/j.jheap.2022.04.002](https://doi.org/10.1016/j.jheap.2022.04.002)

Achitouv, I. 2019, Phys. Rev. D, 100, 123513, doi: [10.1103/PhysRevD.100.123513](https://doi.org/10.1103/PhysRevD.100.123513)

Alam, S., de Mattia, A., Tamone, A., et al. 2021, MNRAS, 504, 4667, doi: [10.1093/mnras/stab1150](https://doi.org/10.1093/mnras/stab1150)

Alcock, C., & Paczynski, B. 1979, Nature, 281, 358, doi: [10.1038/281358a0](https://doi.org/10.1038/281358a0)

Alfaro, I. G., Rodriguez, F., Ruiz, A. N., Loparelo, H. E., & Lambas, D. G. 2022, A&A, 665, A44, doi: [10.1051/0004-6361/202243542](https://doi.org/10.1051/0004-6361/202243542)

Alonso, D., Sanchez, J., Slosar, A., & LSST Dark Energy Science Collaboration. 2019, MNRAS, 484, 4127, doi: [10.1093/mnras/stz093](https://doi.org/10.1093/mnras/stz093)

Angulo, R. E., Baugh, C. M., & Lacey, C. G. 2008, MNRAS, 387, 921, doi: [10.1111/j.1365-2966.2008.13304.x](https://doi.org/10.1111/j.1365-2966.2008.13304.x)

Arsenov, N., Kovács, A., Pérez Sar, M., et al. 2025, arXiv e-prints, arXiv:2509.17696, doi: [10.48550/arXiv.2509.17696](https://doi.org/10.48550/arXiv.2509.17696)

Aubert, M., Cousinou, M.-C., Escoffier, S., et al. 2022, MNRAS, 513, 186, doi: [10.1093/mnras/stac828](https://doi.org/10.1093/mnras/stac828)

Balaguera-Antolínez, A., Montero-Dorta, A. D., & Favole, G. 2024, A&A, 685, A61, doi: [10.1051/0004-6361/202348694](https://doi.org/10.1051/0004-6361/202348694)

Banerjee, A., & Abel, T. 2021, MNRAS, 504, 2911, doi: [10.1093/mnras/stab961](https://doi.org/10.1093/mnras/stab961)

Bardeen, J. M., Bond, J. R., Kaiser, N., & Szalay, A. S. 1986, ApJ, 304, 15, doi: [10.1086/164143](https://doi.org/10.1086/164143)

Basu, K., Hernández-Monteagudo, C., & Sunyaev, R. A. 2004, A&A, 416, 447, doi: [10.1051/0004-6361:20034298](https://doi.org/10.1051/0004-6361:20034298)

Bayer, A. E., Zhong, Y., Li, Z., et al. 2025, J. Cosmology Astropart. Phys., 2025, 016, doi: [10.1088/1475-7516/2025/05/016](https://doi.org/10.1088/1475-7516/2025/05/016)

Behroozi, P., Wechsler, R. H., Hearn, A. P., & Conroy, C. 2019, MNRAS, 488, 3143, doi: [10.1093/mnras/stz1182](https://doi.org/10.1093/mnras/stz1182)

Behroozi, P. S., Wechsler, R. H., & Wu, H.-Y. 2013, ApJ, 762, 109, doi: [10.1088/0004-637X/762/2/109](https://doi.org/10.1088/0004-637X/762/2/109)

Benson, A. 2011, Galacticus: A Semi-Analytic Model of Galaxy Formation, Astrophysics Source Code Library, record ascl:1108.004. <http://ascl.net/1108.004>

Benson, A. J. 2001, MNRAS, 325, 1039, doi: [10.1046/j.1365-8711.2001.04470.x](https://doi.org/10.1046/j.1365-8711.2001.04470.x)

Berlind, A. A., & Weinberg, D. H. 2002a, ApJ, 575, 587, doi: [10.1086/341469](https://doi.org/10.1086/341469)

—. 2002b, ApJ, 575, 587, doi: [10.1086/341469](https://doi.org/10.1086/341469)

Biswas, R., Alizadeh, E., & Wandelt, B. D. 2010, Phys. Rev. D, 82, 023002, doi: [10.1103/PhysRevD.82.023002](https://doi.org/10.1103/PhysRevD.82.023002)

Blanton, M. R., Eisenstein, D., Hogg, D. W., & Zehavi, I. 2006, ApJ, 645, 977, doi: [10.1086/500918](https://doi.org/10.1086/500918)

Blanton, M. R., & Moustakas, J. 2009a, ARA&A, 47, 159, doi: [10.1146/annurev-astro-082708-101734](https://doi.org/10.1146/annurev-astro-082708-101734)

—. 2009b, ARA&A, 47, 159, doi: [10.1146/annurev-astro-082708-101734](https://doi.org/10.1146/annurev-astro-082708-101734)

Bleem, L., Ade, P., Aird, K., et al. 2012, Journal of Low Temperature Physics, 167, 859, doi: [10.1007/s10909-012-0505-y](https://doi.org/10.1007/s10909-012-0505-y)

Bos, E. G. P., van de Weygaert, R., Dolag, K., & Pettorino, V. 2012, MNRAS, 426, 440, doi: [10.1111/j.1365-2966.2012.21478.x](https://doi.org/10.1111/j.1365-2966.2012.21478.x)

Bower, R. G., Benson, A. J., Malbon, R., et al. 2006, MNRAS, 370, 645, doi: [10.1111/j.1365-2966.2006.10519.x](https://doi.org/10.1111/j.1365-2966.2006.10519.x)

Cai, Y.-C., Neyrinck, M., Mao, Q., et al. 2017, MNRAS, 466, 3364, doi: [10.1093/mnras/stw3299](https://doi.org/10.1093/mnras/stw3299)

Cai, Y.-C., Taylor, A., Peacock, J. A., & Padilla, N. 2016, MNRAS, 462, 2465, doi: [10.1093/mnras/stw1809](https://doi.org/10.1093/mnras/stw1809)

Calzetti, D., Armus, L., Bohlin, R. C., et al. 2000, ApJ, 533, 682, doi: [10.1086/308692](https://doi.org/10.1086/308692)

Camacho-Ciurana, G., Lee, P., Arsenov, N., et al. 2024, A&A, 689, A171, doi: [10.1051/0004-6361/202348970](https://doi.org/10.1051/0004-6361/202348970)

Carbone, C., Petkova, M., & Dolag, K. 2016, J. Cosmology Astropart. Phys., 2016, 034, doi: [10.1088/1475-7516/2016/07/034](https://doi.org/10.1088/1475-7516/2016/07/034)

Carlstrom, J. E., Ade, P. A. R., Aird, K. A., et al. 2011, PASP, 123, 568, doi: [10.1086/659879](https://doi.org/10.1086/659879)

Castorina, E., Carbone, C., Bel, J., Sefusatti, E., & Dolag, K. 2015, J. Cosmology Astropart. Phys., 2015, 043, doi: [10.1088/1475-7516/2015/07/043](https://doi.org/10.1088/1475-7516/2015/07/043)

Cautun, M., Paillas, E., Cai, Y.-C., et al. 2018, MNRAS, 476, 3195, doi: [10.1093/mnras/sty463](https://doi.org/10.1093/mnras/sty463)

Chang, C., Omori, Y., Baxter, E. J., et al. 2023, Phys. Rev. D, 107, 023530, doi: [10.1103/PhysRevD.107.023530](https://doi.org/10.1103/PhysRevD.107.023530)

Chantavat, T., Sawangwit, U., Sutter, P. M., & Wandelt, B. D. 2016, Phys. Rev. D, 93, 043523, doi: [10.1103/PhysRevD.93.043523](https://doi.org/10.1103/PhysRevD.93.043523)

Chen, S.-F., Lee, H., & Dvorkin, C. 2021, J. Cosmology Astropart. Phys., 2021, 030, doi: [10.1088/1475-7516/2021/05/030](https://doi.org/10.1088/1475-7516/2021/05/030)

Chuang, C.-H., Yepes, G., Kitaura, F.-S., et al. 2019, MNRAS, 487, 48, doi: [10.1093/mnras/stz1233](https://doi.org/10.1093/mnras/stz1233)

Colberg, J. M., Pearce, F., Foster, C., et al. 2008, MNRAS, 387, 933, doi: [10.1111/j.1365-2966.2008.13307.x](https://doi.org/10.1111/j.1365-2966.2008.13307.x)

Conrado, A. M., González Delgado, R. M., García-Benito, R., et al. 2024, A&A, 687, A98, doi: [10.1051/0004-6361/202449414](https://doi.org/10.1051/0004-6361/202449414)

Conroy, C., Wechsler, R. H., & Kravtsov, A. V. 2006, ApJ, 647, 201, doi: [10.1086/503602](https://doi.org/10.1086/503602)

Contarini, S., Pisani, A., Hamaus, N., et al. 2023, ApJ, 953, 46, doi: [10.3847/1538-4357/acde54](https://doi.org/10.3847/1538-4357/acde54)

—. 2024, A&A, 682, A20, doi: [10.1051/0004-6361/202347572](https://doi.org/10.1051/0004-6361/202347572)

Contarini, S., Ronconi, T., Marulli, F., et al. 2019a, MNRAS, 488, 3526, doi: [10.1093/mnras/stz1989](https://doi.org/10.1093/mnras/stz1989)

—. 2019b, MNRAS, 488, 3526, doi: [10.1093/mnras/stz1989](https://doi.org/10.1093/mnras/stz1989)

Cora, S. A., Vega-Martínez, C. A., Hough, T., et al. 2018, MNRAS, 479, 2, doi: [10.1093/mnras/sty1131](https://doi.org/10.1093/mnras/sty1131)

Correa, C. M., Paz, D. J., Padilla, N. D., et al. 2019, MNRAS, 485, 5761, doi: [10.1093/mnras/stz821](https://doi.org/10.1093/mnras/stz821)

—. 2022a, MNRAS, 509, 1871, doi: [10.1093/mnras/stab3070](https://doi.org/10.1093/mnras/stab3070)

—. 2022b, MNRAS, 509, 1871, doi: [10.1093/mnras/stab3070](https://doi.org/10.1093/mnras/stab3070)

Correa, C. M., Paz, D. J., Sánchez, A. G., et al. 2021a, MNRAS, 500, 911, doi: [10.1093/mnras/staa3252](https://doi.org/10.1093/mnras/staa3252)

—. 2021b, MNRAS, 500, 911, doi: [10.1093/mnras/staa3252](https://doi.org/10.1093/mnras/staa3252)

Dalal, N., White, M., Bond, J. R., & Shirokov, A. 2008, ApJ, 687, 12, doi: [10.1086/591512](https://doi.org/10.1086/591512)

Das, S., Sherwin, B. D., Aguirre, P., et al. 2011, Phys. Rev. Lett., 107, 021301, doi: [10.1103/PhysRevLett.107.021301](https://doi.org/10.1103/PhysRevLett.107.021301)

Degni, G., Sarpa, E., Aubert, M., et al. 2025, arXiv e-prints, arXiv:2509.08884, doi: [10.48550/arXiv.2509.08884](https://doi.org/10.48550/arXiv.2509.08884)

Demirbozan, U., Nadathur, S., Ferrero, I., et al. 2024, MNRAS, 534, 2328, doi: [10.1093/mnras/stae2206](https://doi.org/10.1093/mnras/stae2206)

DESI Collaboration, Aghamousa, A., Aguilar, J., et al. 2016, arXiv e-prints, arXiv:1611.00036, doi: [10.48550/arXiv.1611.00036](https://doi.org/10.48550/arXiv.1611.00036)

Dolag, K., Komatsu, E., & Sunyaev, R. 2016, MNRAS, 463, 1797, doi: [10.1093/mnras/stw2035](https://doi.org/10.1093/mnras/stw2035)

Domínguez-Gómez, J., Pérez, I., Ruiz-Lara, T., et al. 2023, Nature, 619, 269, doi: [10.1038/s41586-023-06109-1](https://doi.org/10.1038/s41586-023-06109-1)

Dubois, Y., Pichon, C., Welker, C., et al. 2014a, MNRAS, 444, 1453, doi: [10.1093/mnras/stu1227](https://doi.org/10.1093/mnras/stu1227)

—. 2014b, MNRAS, 444, 1453, doi: [10.1093/mnras/stu1227](https://doi.org/10.1093/mnras/stu1227)

—. 2014c, MNRAS, 444, 1453, doi: [10.1093/mnras/stu1227](https://doi.org/10.1093/mnras/stu1227)

Efstathiou, G. 2025, Philosophical Transactions of the Royal Society of London Series A, 383, 20240022, doi: [10.1098/rsta.2024.0022](https://doi.org/10.1098/rsta.2024.0022)

Faltenbacher, A., & White, S. D. M. 2010, ApJ, 708, 469, doi: [10.1088/0004-637X/708/1/469](https://doi.org/10.1088/0004-637X/708/1/469)

Fang, Y., Hamaus, N., Jain, B., et al. 2019, MNRAS, 490, 3573, doi: [10.1093/mnras/stz2805](https://doi.org/10.1093/mnras/stz2805)

Favole, G., Comparat, J., Prada, F., et al. 2016, MNRAS, 461, 3421, doi: [10.1093/mnras/stw1483](https://doi.org/10.1093/mnras/stw1483)

Fernández-García, E., Betancort-Rijo, J. E., Prada, F., et al. 2025, A&A, 695, A19, doi: [10.1051/0004-6361/202451264](https://doi.org/10.1051/0004-6361/202451264)

Fraser, T. S., Paillas, E., Percival, W. J., et al. 2025, J. Cosmology Astropart. Phys., 2025, 001, doi: [10.1088/1475-7516/2025/06/001](https://doi.org/10.1088/1475-7516/2025/06/001)

Fry, J. N. 1996, ApJ, 461, L65, doi: [10.1086/310006](https://doi.org/10.1086/310006)

Furlanetto, S. R., & Piran, T. 2006, MNRAS, 366, 467, doi: [10.1111/j.1365-2966.2005.09862.x](https://doi.org/10.1111/j.1365-2966.2005.09862.x)

Gao, L., Springel, V., & White, S. D. M. 2005, MNRAS, 363, L66, doi: [10.1111/j.1745-3933.2005.00084.x](https://doi.org/10.1111/j.1745-3933.2005.00084.x)

Geach, J. E., Smail, I., Best, P. N., et al. 2008, MNRAS, 388, 1473, doi: [10.1111/j.1365-2966.2008.13481.x](https://doi.org/10.1111/j.1365-2966.2008.13481.x)

Gonzalez-Perez, V., Cui, W., Contreras, S., et al. 2020, MNRAS, 498, 1852, doi: [10.1093/mnras/staa2504](https://doi.org/10.1093/mnras/staa2504)

Górski, K. M., Hivon, E., Banday, A. J., et al. 2005, *ApJ*, 622, 759, doi: [10.1086/427976](https://doi.org/10.1086/427976)

Green, J., Schechter, P., Baltay, C., et al. 2012, arXiv e-prints, arXiv:1208.4012, doi: [10.48550/arXiv.1208.4012](https://doi.org/10.48550/arXiv.1208.4012)

Gregory, S. A., & Thompson, L. A. 1978, *ApJ*, 222, 784, doi: [10.1086/156198](https://doi.org/10.1086/156198)

Guo, H., Zheng, Z., Zehavi, I., et al. 2015, *MNRAS*, 453, 4368, doi: [10.1093/mnras/stv1966](https://doi.org/10.1093/mnras/stv1966)

Hadzhiyska, B., Bose, S., Eisenstein, D., Hernquist, L., & Spergel, D. N. 2020, *MNRAS*, 493, 5506, doi: [10.1093/mnras/staa623](https://doi.org/10.1093/mnras/staa623)

Hahn, O., Porciani, C., Carollo, C. M., & Dekel, A. 2007, *MNRAS*, 375, 489, doi: [10.1111/j.1365-2966.2006.11318.x](https://doi.org/10.1111/j.1365-2966.2006.11318.x)

Hamaus, N., Pisani, A., Choi, J.-A., et al. 2020, *J. Cosmology Astropart. Phys.*, 2020, 023, doi: [10.1088/1475-7516/2020/12/023](https://doi.org/10.1088/1475-7516/2020/12/023)

Hamaus, N., Sutter, P. M., Lavaux, G., & Wandelt, B. D. 2015, *J. Cosmology Astropart. Phys.*, 2015, 036, doi: [10.1088/1475-7516/2015/11/036](https://doi.org/10.1088/1475-7516/2015/11/036)

Hamaus, N., Sutter, P. M., & Wandelt, B. D. 2014, *Phys. Rev. Lett.*, 112, 251302, doi: [10.1103/PhysRevLett.112.251302](https://doi.org/10.1103/PhysRevLett.112.251302)

Hamaus, N., Aubert, M., Pisani, A., et al. 2022, *A&A*, 658, A20, doi: [10.1051/0004-6361/202142073](https://doi.org/10.1051/0004-6361/202142073)

Han, J., Li, Y., Jing, Y., et al. 2019a, *MNRAS*, 482, 1900, doi: [10.1093/mnras/sty2822](https://doi.org/10.1093/mnras/sty2822)

—. 2019b, *MNRAS*, 482, 1900, doi: [10.1093/mnras/sty2822](https://doi.org/10.1093/mnras/sty2822)

Hang, Q., Alam, S., Cai, Y.-C., & Peacock, J. A. 2021, *MNRAS*, 507, 510, doi: [10.1093/mnras/stab2184](https://doi.org/10.1093/mnras/stab2184)

Hawken, A. J., Granett, B. R., Iovino, A., et al. 2017, *A&A*, 607, A54, doi: [10.1051/0004-6361/201629678](https://doi.org/10.1051/0004-6361/201629678)

Hearin, A., Korytov, D., Kovacs, E., et al. 2020, *MNRAS*, 495, 5040, doi: [10.1093/mnras/staa1495](https://doi.org/10.1093/mnras/staa1495)

Hearin, A. P., Watson, D. F., Becker, M. R., et al. 2014, *MNRAS*, 444, 729, doi: [10.1093/mnras/stu1443](https://doi.org/10.1093/mnras/stu1443)

Hernández-Monteagudo, C. 2019, in *Highlights on Spanish Astrophysics X*, ed. B. Montesinos, A. Asensio Ramos, F. Buitrago, R. Schödel, E. Villaver, S. Pérez-Hoyos, & I. Ordóñez-Etxeberria, 134–139

Hernández-Monteagudo, C., Rubiño-Martín, J. A., & Sunyaev, R. A. 2007, *MNRAS*, 380, 1656, doi: [10.1111/j.1365-2966.2007.12218.x](https://doi.org/10.1111/j.1365-2966.2007.12218.x)

Hernández-Monteagudo, C., Verde, L., & Jimenez, R. 2006, *ApJ*, 653, 1, doi: [10.1086/508529](https://doi.org/10.1086/508529)

Hirata, C. M., Ho, S., Padmanabhan, N., Seljak, U., & Bahcall, N. A. 2008, *Phys. Rev. D*, 78, 043520, doi: [10.1103/PhysRevD.78.043520](https://doi.org/10.1103/PhysRevD.78.043520)

Ho, S., Hirata, C., Padmanabhan, N., Seljak, U., & Bahcall, N. 2008, *Phys. Rev. D*, 78, 043519, doi: [10.1103/PhysRevD.78.043519](https://doi.org/10.1103/PhysRevD.78.043519)

Jøeveer, M., Einasto, J., & Tago, E. 1978, *MNRAS*, 185, 357, doi: [10.1093/mnras/185.2.357](https://doi.org/10.1093/mnras/185.2.357)

Jeffrey, N., Whiteway, L., Gatti, M., et al. 2025, *MNRAS*, 536, 1303, doi: [10.1093/mnras/stae2629](https://doi.org/10.1093/mnras/stae2629)

Jennings, E., Li, Y., & Hu, W. 2013a, *MNRAS*, 434, 2167, doi: [10.1093/mnras/stt1169](https://doi.org/10.1093/mnras/stt1169)

—. 2013b, *MNRAS*, 434, 2167, doi: [10.1093/mnras/stt1169](https://doi.org/10.1093/mnras/stt1169)

Kaiser, N. 1984, *ApJ*, 284, L9, doi: [10.1086/184341](https://doi.org/10.1086/184341)

—. 1987, *MNRAS*, 227, 1, doi: [10.1093/mnras/227.1.1](https://doi.org/10.1093/mnras/227.1.1)

Kauffmann, G., White, S. D. M., Heckman, T. M., et al. 2004, *MNRAS*, 353, 713, doi: [10.1111/j.1365-2966.2004.08117.x](https://doi.org/10.1111/j.1365-2966.2004.08117.x)

Klypin, A., Yepes, G., Gottlöber, S., Prada, F., & Heß, S. 2016, *MNRAS*, 457, 4340, doi: [10.1093/mnras/stw248](https://doi.org/10.1093/mnras/stw248)

Knox, L. 1995, *Phys. Rev. D*, 52, 4307, doi: [10.1103/PhysRevD.52.4307](https://doi.org/10.1103/PhysRevD.52.4307)

Kovács, A., Vielzeuf, P., Ferrero, I., et al. 2022, *MNRAS*, 515, 4417, doi: [10.1093/mnras/stac2011](https://doi.org/10.1093/mnras/stac2011)

Krolewski, A., Ferraro, S., & White, M. 2021, *J. Cosmology Astropart. Phys.*, 2021, 028, doi: [10.1088/1475-7516/2021/12/028](https://doi.org/10.1088/1475-7516/2021/12/028)

Landy, S. D., & Szalay, A. S. 1993, *ApJ*, 412, 64, doi: [10.1086/172900](https://doi.org/10.1086/172900)

Laureijs, R., Amiaux, J., Arduini, S., et al. 2011, arXiv e-prints, arXiv:1110.3193, doi: [10.48550/arXiv.1110.3193](https://doi.org/10.48550/arXiv.1110.3193)

Lavaux, G., & Wandelt, B. D. 2010, *MNRAS*, 403, 1392, doi: [10.1111/j.1365-2966.2010.16197.x](https://doi.org/10.1111/j.1365-2966.2010.16197.x)

—. 2012, *ApJ*, 754, 109, doi: [10.1088/0004-637X/754/2/109](https://doi.org/10.1088/0004-637X/754/2/109)

Lazeyras, T., Musso, M., & Schmidt, F. 2017, *J. Cosmology Astropart. Phys.*, 2017, 059, doi: [10.1088/1475-7516/2017/03/059](https://doi.org/10.1088/1475-7516/2017/03/059)

Lewis, A. 2013, *J. Cosmology Astropart. Phys.*, 2013, 053, doi: [10.1088/1475-7516/2013/08/053](https://doi.org/10.1088/1475-7516/2013/08/053)

Lewis, A., & Challinor, A. 2006, *Phys. Rep.*, 429, 1, doi: [10.1016/j.physrep.2006.03.002](https://doi.org/10.1016/j.physrep.2006.03.002)

Li, Y., Mo, H. J., & Gao, L. 2008, *MNRAS*, 389, 1419, doi: [10.1111/j.1365-2966.2008.13667.x](https://doi.org/10.1111/j.1365-2966.2008.13667.x)

Mao, Q., Berlind, A. A., Scherrer, R. J., et al. 2017, *ApJ*, 835, 160, doi: [10.3847/1538-4357/835/2/160](https://doi.org/10.3847/1538-4357/835/2/160)

Mauland, R., Elgaroy, Ø., Mota, D. F., & Winther, H. A. 2023, *A&A*, 674, A185, doi: [10.1051/0004-6361/202346287](https://doi.org/10.1051/0004-6361/202346287)

McCarthy, I. G., Schaye, J., Bird, S., & Le Brun, A. M. C. 2017, *MNRAS*, 465, 2936, doi: [10.1093/mnras/stw2792](https://doi.org/10.1093/mnras/stw2792)

Mo, H. J., & White, S. D. M. 1996, *MNRAS*, 282, 347, doi: [10.1093/mnras/282.2.347](https://doi.org/10.1093/mnras/282.2.347)

Montero-Dorta, A. D., Chaves-Montero, J., Artale, M. C., & Favole, G. 2021, *MNRAS*, 508, 940, doi: [10.1093/mnras/stab2556](https://doi.org/10.1093/mnras/stab2556)

Moresco, M., Amati, L., Amendola, L., et al. 2022, *Living Reviews in Relativity*, 25, 6, doi: [10.1007/s41114-022-00040-z](https://doi.org/10.1007/s41114-022-00040-z)

Moster, B. P., Naab, T., & White, S. D. M. 2013, *MNRAS*, 428, 3121, doi: [10.1093/mnras/sts261](https://doi.org/10.1093/mnras/sts261)

—. 2018, *MNRAS*, 477, 1822, doi: [10.1093/mnras/sty655](https://doi.org/10.1093/mnras/sty655)

Moster, B. P., Somerville, R. S., Maulbetsch, C., et al. 2010, *ApJ*, 710, 903, doi: [10.1088/0004-637X/710/2/903](https://doi.org/10.1088/0004-637X/710/2/903)

Nadathur, S., Carter, P., & Percival, W. J. 2019a, *MNRAS*, 482, 2459, doi: [10.1093/mnras/sty2799](https://doi.org/10.1093/mnras/sty2799)

Nadathur, S., Carter, P. M., Percival, W. J., Winther, H. A., & Bautista, J. E. 2019b, *Phys. Rev. D*, 100, 023504, doi: [10.1103/PhysRevD.100.023504](https://doi.org/10.1103/PhysRevD.100.023504)

Nadathur, S., & Hotchkiss, S. 2015a, *MNRAS*, 454, 889, doi: [10.1093/mnras/stv194](https://doi.org/10.1093/mnras/stv194)

—. 2015b, *MNRAS*, 454, 2228, doi: [10.1093/mnras/stv2131](https://doi.org/10.1093/mnras/stv2131)

Nadathur, S., Woodfinden, A., Percival, W. J., et al. 2020, *MNRAS*, 499, 4140, doi: [10.1093/mnras/staa3074](https://doi.org/10.1093/mnras/staa3074)

Neyrinck, M. C. 2008, *MNRAS*, 386, 2101, doi: [10.1111/j.1365-2966.2008.13180.x](https://doi.org/10.1111/j.1365-2966.2008.13180.x)

Nicola, A., Refregier, A., & Amara, A. 2016, *Phys. Rev. D*, 94, 083517, doi: [10.1103/PhysRevD.94.083517](https://doi.org/10.1103/PhysRevD.94.083517)

Observations Time Allocation Committee, R., & Community Survey Definition Committees, C. 2025, arXiv e-prints, arXiv:2505.10574, doi: [10.48550/arXiv.2505.10574](https://doi.org/10.48550/arXiv.2505.10574)

Omori, Y. 2024, *MNRAS*, 530, 5030, doi: [10.1093/mnras/stae1031](https://doi.org/10.1093/mnras/stae1031)

Omori, Y., Baxter, E. J., Chang, C., et al. 2023, *Phys. Rev. D*, 107, 023529, doi: [10.1103/PhysRevD.107.023529](https://doi.org/10.1103/PhysRevD.107.023529)

Paillas, E., Cai, Y.-C., Padilla, N., & Sánchez, A. G. 2021, *MNRAS*, 505, 5731, doi: [10.1093/mnras/stab1654](https://doi.org/10.1093/mnras/stab1654)

Paillas, E., Cautun, M., Li, B., et al. 2019, *MNRAS*, 484, 1149, doi: [10.1093/mnras/stz022](https://doi.org/10.1093/mnras/stz022)

Paillas, E., Lagos, C. D. P., Padilla, N., et al. 2017, *MNRAS*, 470, 4434, doi: [10.1093/mnras/stx1514](https://doi.org/10.1093/mnras/stx1514)

Paranjape, A., Hahn, O., & Sheth, R. K. 2018, *MNRAS*, 476, 5442, doi: [10.1093/mnras/sty633](https://doi.org/10.1093/mnras/sty633)

Paviot, R., Rocher, A., Codis, S., et al. 2024, *A&A*, 690, A221, doi: [10.1051/0004-6361/202449574](https://doi.org/10.1051/0004-6361/202449574)

Paz, D. J., Correia, C. M., Gualpa, S. R., et al. 2023, *MNRAS*, 522, 2553, doi: [10.1093/mnras/stad1146](https://doi.org/10.1093/mnras/stad1146)

Peacock, J. A., & Smith, R. E. 2000, *MNRAS*, 318, 1144, doi: [10.1046/j.1365-8711.2000.03779.x](https://doi.org/10.1046/j.1365-8711.2000.03779.x)

Pearson, R., & Zahn, O. 2014, *Phys. Rev. D*, 89, 043516, doi: [10.1103/PhysRevD.89.043516](https://doi.org/10.1103/PhysRevD.89.043516)

Pedregosa, F., Varoquaux, G., Gramfort, A., et al. 2011, *Journal of Machine Learning Research*, 12, 2825, doi: [10.48550/arXiv.1201.0490](https://doi.org/10.48550/arXiv.1201.0490)

Peebles, P. J. E. 2022, *Annals of Physics*, 447, 169159, doi: [10.1016/j.aop.2022.169159](https://doi.org/10.1016/j.aop.2022.169159)

Pelliciari, D., Contarini, S., Marulli, F., et al. 2023, *MNRAS*, 522, 152, doi: [10.1093/mnras/stad956](https://doi.org/10.1093/mnras/stad956)

Perez, L. A., Genel, S., Villaescusa-Navarro, F., et al. 2023, *ApJ*, 954, 11, doi: [10.3847/1538-4357/accd52](https://doi.org/10.3847/1538-4357/accd52)

Perivolaropoulos, L., & Skara, F. 2022, *New A Rev.*, 95, 101659, doi: [10.1016/j.newar.2022.101659](https://doi.org/10.1016/j.newar.2022.101659)

Pisani, A., Lavaux, G., Sutter, P. M., & Wandelt, B. D. 2014, *MNRAS*, 443, 3238, doi: [10.1093/mnras/stu1399](https://doi.org/10.1093/mnras/stu1399)

Pisani, A., Sutter, P. M., Hamaus, N., et al. 2015, *Phys. Rev. D*, 92, 083531, doi: [10.1103/PhysRevD.92.083531](https://doi.org/10.1103/PhysRevD.92.083531)

Pisani, A., Massara, E., Spergel, D. N., et al. 2019, *BAAS*, 51, 40, doi: [10.48550/arXiv.1903.05161](https://doi.org/10.48550/arXiv.1903.05161)

Planck Collaboration, Ade, P. A. R., Aghanim, N., et al. 2014, *A&A*, 571, A17, doi: [10.1051/0004-6361/201321543](https://doi.org/10.1051/0004-6361/201321543)

—. 2016a, *A&A*, 594, A15, doi: [10.1051/0004-6361/201525941](https://doi.org/10.1051/0004-6361/201525941)

—. 2016b, *A&A*, 594, A13, doi: [10.1051/0004-6361/201525830](https://doi.org/10.1051/0004-6361/201525830)

Planck Collaboration, Aghanim, N., Akrami, Y., et al. 2020, *A&A*, 641, A6, doi: [10.1051/0004-6361/201833910](https://doi.org/10.1051/0004-6361/201833910)

Platen, E., van de Weygaert, R., & Jones, B. J. T. 2007, *MNRAS*, 380, 551, doi: [10.1111/j.1365-2966.2007.12125.x](https://doi.org/10.1111/j.1365-2966.2007.12125.x)

Pollina, G., Baldi, M., Marulli, F., & Moscardini, L. 2016, *MNRAS*, 455, 3075, doi: [10.1093/mnras/stv2503](https://doi.org/10.1093/mnras/stv2503)

Pujol, A., Hoffmann, K., Jiménez, N., & Gaztañaga, E. 2017, *A&A*, 598, A103, doi: [10.1051/0004-6361/201629121](https://doi.org/10.1051/0004-6361/201629121)

Radinović, S., Nadathur, S., Winther, H. A., et al. 2023, *A&A*, 677, A78, doi: [10.1051/0004-6361/202346121](https://doi.org/10.1051/0004-6361/202346121)

Raghunathan, S., Nadathur, S., Sherwin, B. D., & Whitehorn, N. 2020, *ApJ*, 890, 168, doi: [10.3847/1538-4357/ab6f05](https://doi.org/10.3847/1538-4357/ab6f05)

Ramakrishnan, S., Paranjape, A., Hahn, O., & Sheth, R. K. 2019, MNRAS, 489, 2977, doi: [10.1093/mnras/stz2344](https://doi.org/10.1093/mnras/stz2344)

Rocher, A., Ruhlmann-Kleider, V., Burtin, E., et al. 2023, J. Cosmology Astropart. Phys., 2023, 016, doi: [10.1088/1475-7516/2023/10/016](https://doi.org/10.1088/1475-7516/2023/10/016)

Rodriguez, F., Merchán, M., & Sgró, M. A. 2015, A&A, 580, A86, doi: [10.1051/0004-6361/201525798](https://doi.org/10.1051/0004-6361/201525798)

Ronconi, T., & Marulli, F. 2017, A&A, 607, A24, doi: [10.1051/0004-6361/201730852](https://doi.org/10.1051/0004-6361/201730852)

Ryden, B. S. 1995, ApJ, 452, 25, doi: [10.1086/176277](https://doi.org/10.1086/176277)

Ryden, B. S., & Melott, A. L. 1996, ApJ, 470, 160, doi: [10.1086/177857](https://doi.org/10.1086/177857)

Sachs, R. K., & Wolfe, A. M. 1967, ApJ, 147, 73, doi: [10.1086/148982](https://doi.org/10.1086/148982)

Salcedo, A. N., Maller, A. H., Berlind, A. A., et al. 2018, MNRAS, 475, 4411, doi: [10.1093/mnras/sty109](https://doi.org/10.1093/mnras/sty109)

Salcedo, A. N., Pisani, A., & Hamaus, N. 2025, arXiv e-prints, arXiv:2504.08221, doi: [10.48550/arXiv.2504.08221](https://doi.org/10.48550/arXiv.2504.08221)

Sánchez, C., Clampitt, J., Kovacs, A., et al. 2017, MNRAS, 465, 746, doi: [10.1093/mnras/stw2745](https://doi.org/10.1093/mnras/stw2745)

Sartori, S., Vielzeuf, P., Escouffier, S., et al. 2025, A&A, 700, A17, doi: [10.1051/0004-6361/202453562](https://doi.org/10.1051/0004-6361/202453562)

Sato-Polito, G., Kokron, N., & Bernal, J. L. 2023a, MNRAS, 526, 5883, doi: [10.1093/mnras/stad2498](https://doi.org/10.1093/mnras/stad2498)

—. 2023b, MNRAS, 526, 5883, doi: [10.1093/mnras/stad2498](https://doi.org/10.1093/mnras/stad2498)

Sato-Polito, G., Montero-Dorta, A. D., Abramo, L. R., Prada, F., & Klypin, A. 2019, MNRAS, 487, 1570, doi: [10.1093/mnras/stz1338](https://doi.org/10.1093/mnras/stz1338)

Schaller, M., Frenk, C. S., Bower, R. G., et al. 2015, MNRAS, 451, 1247, doi: [10.1093/mnras/stv1067](https://doi.org/10.1093/mnras/stv1067)

Schaye, J., Kugel, R., Schaller, M., et al. 2023, MNRAS, 526, 4978, doi: [10.1093/mnras/stad2419](https://doi.org/10.1093/mnras/stad2419)

Schuster, N., Hamaus, N., Pisani, A., Dolag, K., & Weller, J. 2025, arXiv e-prints, arXiv:2509.07092, doi: [10.48550/arXiv.2509.07092](https://doi.org/10.48550/arXiv.2509.07092)

Shaikh, S., Harrison, I., van Engelen, A., et al. 2024, MNRAS, 528, 2112, doi: [10.1093/mnras/stad3987](https://doi.org/10.1093/mnras/stad3987)

Sherwin, B. D., van Engelen, A., Sehgal, N., et al. 2017, Phys. Rev. D, 95, 123529, doi: [10.1103/PhysRevD.95.123529](https://doi.org/10.1103/PhysRevD.95.123529)

Sheth, R. K., & Tormen, G. 2004, MNRAS, 350, 1385, doi: [10.1111/j.1365-2966.2004.07733.x](https://doi.org/10.1111/j.1365-2966.2004.07733.x)

Sheth, R. K., & van de Weygaert, R. 2004a, MNRAS, 350, 517, doi: [10.1111/j.1365-2966.2004.07661.x](https://doi.org/10.1111/j.1365-2966.2004.07661.x)

—. 2004b, MNRAS, 350, 517, doi: [10.1111/j.1365-2966.2004.07661.x](https://doi.org/10.1111/j.1365-2966.2004.07661.x)

Shirasaki, M., Hamana, T., & Yoshida, N. 2015, MNRAS, 453, 3043, doi: [10.1093/mnras/stv1854](https://doi.org/10.1093/mnras/stv1854)

Sinha, M., & Garrison, L. H. 2020, MNRAS, 491, 3022, doi: [10.1093/mnras/stz3157](https://doi.org/10.1093/mnras/stz3157)

Sobral, D., Smail, I., Best, P. N., et al. 2013, MNRAS, 428, 1128, doi: [10.1093/mnras/sts096](https://doi.org/10.1093/mnras/sts096)

Sobral, D., Best, P. N., Geach, J. E., et al. 2009, MNRAS, 398, 75, doi: [10.1111/j.1365-2966.2009.15129.x](https://doi.org/10.1111/j.1365-2966.2009.15129.x)

Somerville, R. S., & Davé, R. 2015, ARA&A, 53, 51, doi: [10.1146/annurev-astro-082812-140951](https://doi.org/10.1146/annurev-astro-082812-140951)

Song, Y., Xiong, Q., Gong, Y., et al. 2024, MNRAS, 532, 1049, doi: [10.1093/mnras/stae1575](https://doi.org/10.1093/mnras/stae1575)

Spergel, D., Gehrels, N., Baltay, C., et al. 2015a, arXiv e-prints, arXiv:1503.03757, doi: [10.48550/arXiv.1503.03757](https://doi.org/10.48550/arXiv.1503.03757)

—. 2015b, arXiv e-prints, arXiv:1503.03757, doi: [10.48550/arXiv.1503.03757](https://doi.org/10.48550/arXiv.1503.03757)

Springel, V., Pakmor, R., Pillepich, A., et al. 2018, MNRAS, 475, 676, doi: [10.1093/mnras/stx3304](https://doi.org/10.1093/mnras/stx3304)

Stein, G., Alvarez, M. A., Bond, J. R., van Engelen, A., & Battaglia, N. 2020, J. Cosmology Astropart. Phys., 2020, 012, doi: [10.1088/1475-7516/2020/10/012](https://doi.org/10.1088/1475-7516/2020/10/012)

Story, K. T., Hanson, D., Ade, P. A. R., et al. 2015, ApJ, 810, 50, doi: [10.1088/0004-637X/810/1/50](https://doi.org/10.1088/0004-637X/810/1/50)

Sunyaev, R. A., & Zeldovich, I. B. 1980, MNRAS, 190, 413

Sunyaev, R. A., & Zeldovich, Y. B. 1972, Comments on Astrophysics and Space Physics, 4, 173

Sutter, P. M., Lavaux, G., Wandelt, B. D., & Weinberg, D. H. 2012, ApJ, 761, 187, doi: [10.1088/0004-637X/761/2/187](https://doi.org/10.1088/0004-637X/761/2/187)

Sutter, P. M., Lavaux, G., Wandelt, B. D., Weinberg, D. H., & Warren, M. S. 2014a, MNRAS, 438, 3177, doi: [10.1093/mnras/stt2425](https://doi.org/10.1093/mnras/stt2425)

—. 2014b, MNRAS, 438, 3177, doi: [10.1093/mnras/stt2425](https://doi.org/10.1093/mnras/stt2425)

Sutter, P. M., Lavaux, G., Wandelt, B. D., et al. 2014c, MNRAS, 442, 3127, doi: [10.1093/mnras/stu1094](https://doi.org/10.1093/mnras/stu1094)

Tacchella, S., Bose, S., Conroy, C., Eisenstein, D. J., & Johnson, B. D. 2018, ApJ, 868, 92, doi: [10.3847/1538-4357/aae8e0](https://doi.org/10.3847/1538-4357/aae8e0)

Tacchella, S., Trenti, M., & Carollo, C. M. 2013, ApJ, 768, L37, doi: [10.1088/2041-8205/768/2/L37](https://doi.org/10.1088/2041-8205/768/2/L37)

Tegmark, M., & Peebles, P. J. E. 1998, ApJ, 500, L79, doi: [10.1086/311426](https://doi.org/10.1086/311426)

The Planck Collaboration. 2006, arXiv e-prints, astro, doi: [10.48550/arXiv.astro-ph/0604069](https://doi.org/10.48550/arXiv.astro-ph/0604069)

Tinker, J. L., Weinberg, D. H., & Warren, M. S. 2006a, ApJ, 647, 737, doi: [10.1086/504795](https://doi.org/10.1086/504795)

—. 2006b, ApJ, 647, 737, doi: [10.1086/504795](https://doi.org/10.1086/504795)

Troxel, M. A., & Ishak, M. 2014, Phys. Rev. D, 89, 063528, doi: [10.1103/PhysRevD.89.063528](https://doi.org/10.1103/PhysRevD.89.063528)

Tucci, B., Montero-Dorta, A. D., Abramo, L. R., Sato-Polito, G., & Artale, M. C. 2021, MNRAS, 500, 2777, doi: [10.1093/mnras/staa3319](https://doi.org/10.1093/mnras/staa3319)

Verza, G., Carbone, C., Pisani, A., Porciani, C., & Matarrese, S. 2024a, J. Cosmology Astropart. Phys., 2024, 079, doi: [10.1088/1475-7516/2024/10/079](https://doi.org/10.1088/1475-7516/2024/10/079)

Verza, G., Degni, G., Pisani, A., et al. 2024b, arXiv e-prints, arXiv:2410.19713, doi: [10.48550/arXiv.2410.19713](https://doi.org/10.48550/arXiv.2410.19713)

—. 2024c, arXiv e-prints, arXiv:2410.19713, doi: [10.48550/arXiv.2410.19713](https://doi.org/10.48550/arXiv.2410.19713)

Vielzeuf, P., Kovács, A., Demirbozan, U., et al. 2021a, MNRAS, 500, 464, doi: [10.1093/mnras/staa3231](https://doi.org/10.1093/mnras/staa3231)

—. 2021b, MNRAS, 500, 464, doi: [10.1093/mnras/staa3231](https://doi.org/10.1093/mnras/staa3231)

Villaescusa-Navarro, F., Anglés-Alcázar, D., Genel, S., et al. 2021, ApJ, 915, 71, doi: [10.3847/1538-4357/abf7ba](https://doi.org/10.3847/1538-4357/abf7ba)

Virtanen, P., Gommers, R., Oliphant, T. E., et al. 2020, Nature Methods, 17, 261, doi: [10.1038/s41592-019-0686-2](https://doi.org/10.1038/s41592-019-0686-2)

Wang, Y., Zhai, Z., Alavi, A., et al. 2022, ApJ, 928, 1, doi: [10.3847/1538-4357/ac4973](https://doi.org/10.3847/1538-4357/ac4973)

Wechsler, R. H., DeRose, J., Busha, M. T., et al. 2022, ApJ, 931, 145, doi: [10.3847/1538-4357/ac5b0a](https://doi.org/10.3847/1538-4357/ac5b0a)

Wechsler, R. H., & Tinker, J. L. 2018, ARA&A, 56, 435, doi: [10.1146/annurev-astro-081817-051756](https://doi.org/10.1146/annurev-astro-081817-051756)

Wechsler, R. H., Zentner, A. R., Bullock, J. S., Kravtsov, A. V., & Allgood, B. 2006, ApJ, 652, 71, doi: [10.1086/507120](https://doi.org/10.1086/507120)

White, S. D. M., & Rees, M. J. 1978, MNRAS, 183, 341, doi: [10.1093/mnras/183.3.341](https://doi.org/10.1093/mnras/183.3.341)

Woodfinden, A., Nadathur, S., Percival, W. J., et al. 2022, MNRAS, 516, 4307, doi: [10.1093/mnras/stac2475](https://doi.org/10.1093/mnras/stac2475)

Wu, J. F., Jespersen, C. K., & Wechsler, R. H. 2024, ApJ, 976, 37, doi: [10.3847/1538-4357/ad7bb3](https://doi.org/10.3847/1538-4357/ad7bb3)

Wu, W. L. K., Mocanu, L. M., Ade, P. A. R., et al. 2019, ApJ, 884, 70, doi: [10.3847/1538-4357/ab4186](https://doi.org/10.3847/1538-4357/ab4186)

Yu, J., Zhao, C., Gonzalez-Perez, V., et al. 2024, MNRAS, 527, 6950, doi: [10.1093/mnras/stad3559](https://doi.org/10.1093/mnras/stad3559)

Yuan, S., Garrison, L. H., Hadzhiyska, B., Bose, S., & Eisenstein, D. J. 2022, MNRAS, 510, 3301, doi: [10.1093/mnras/stab3355](https://doi.org/10.1093/mnras/stab3355)

Yuan, S., Hadzhiyska, B., Bose, S., Eisenstein, D. J., & Guo, H. 2021, MNRAS, 502, 3582, doi: [10.1093/mnras/stab235](https://doi.org/10.1093/mnras/stab235)

Yuan, S., Wechsler, R. H., Wang, Y., et al. 2025, MNRAS, 538, 1216, doi: [10.1093/mnras/staf368](https://doi.org/10.1093/mnras/staf368)

Zhai, Z., Chuang, C.-H., Wang, Y., Benson, A., & Yepes, G. 2021, MNRAS, 501, 3490, doi: [10.1093/mnras/staa3911](https://doi.org/10.1093/mnras/staa3911)

Zheng, Z., Berlind, A. A., Weinberg, D. H., et al. 2005, ApJ, 633, 791, doi: [10.1086/466510](https://doi.org/10.1086/466510)

Appendix A: Sensitivity of void finder to sub/over-sampling of particles

Since we have applied a minimum halo mass cut in the reference catalog to equalize the resolution of the simulations, we test the sensitivity of the two void finders to small changes in the galaxy population. The left side of Fig. A.1 (to the left of the zero on the x -axis) represents subsampling of the physical tracer particles in the mock catalog, while the right side illustrates the addition of fake galaxies to the mock catalog.

The observed trends depend not only on subsampling or over-sampling but also on the specific void finder used. In the case of subsampling, the 3D void finder detects fewer voids than the nominal case, with the voids being typically larger due to the increase in the volume of voids devoid of matter. In contrast, for the over-sampling case, the random distribution of galaxies causes the fragmentation of some nominal voids into smaller ones.

The 2D void finder shows less sensitivity to these changes. When real galaxies are removed, the number of voids remains relatively unchanged. However, when random galaxies are added, the behavior differs from that of the 3D void finder. Due to the 2D void finder’s projected nature, the overall mean density across the map increases, which leads to the identification of fewer voids (only the biggest and deeper ones).

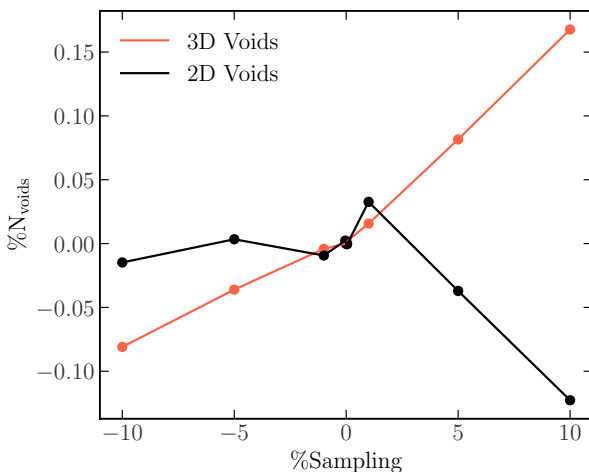


Fig. A.1: Sensitivity of 3D and 2D void finders to under- and over-sampling the tracer galaxy field.

In our case, a decrease of 1.34% of the tracer galaxies will induce a change in the number of voids of 0.05% which we consider negligible.

In this test, we specifically vary the number density of galaxies, which, as expected, results in changes in the number of voids. What is, however, particularly interesting—and something that was not thoroughly addressed in prior work, except for Tinker et al. (2006a)—is that even when the number density of galaxies and the power spectra are identical, this does not necessarily lead to the same void statistics as seen in Figure D.1. This highlights the need to examine these statistics when generating mock catalogs for void-based analyses or more precise and consistent galaxy analysis.

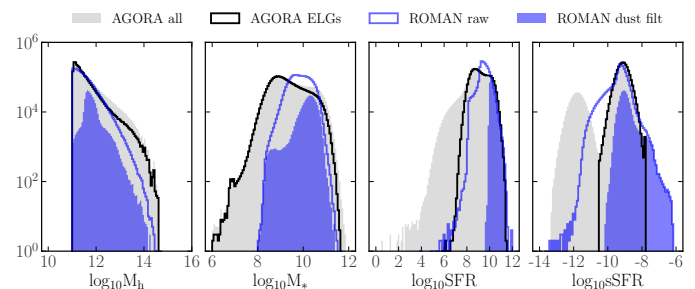


Fig. B.1: Distribution of halo mass, stellar mass, star formation rate, and specific star formation rate in AGORA (derived from UNIVERSE MACHINE) and the reference catalog (derived from GALACTICUS).

Appendix B: Different calibration of M_* and SFR for Roman reference catalog and the Agora simulation

In Figure B.1, we compare, for a redshift slice around $z = 1.1$, the host-halo mass and baryonic properties derived from UNIVERSE MACHINE (for AGORA) and GALACTICUS (for the ROMAN reference catalog). We present the distributions for the full AGORA halo population alongside the flagged ELGs—identified via the characteristic bimodal sSFR distribution—and compare these to the raw and dust-filtered versions of the ROMAN reference mock catalog. While ROMAN exhibit a slight systematic shift toward higher M_* and sSFR, our analysis demonstrates that these offsets do not significantly impact the analog matching’s ability to recover the expected clustering bias of the ROMAN ELG sample.

Appendix C: Void statistics for 2D void finder with $sm_{VF} = 5 h^{-1} \text{Mpc}$

Figure C.1 shows the one- and two-point statistics for 2D voids identified with a void-finder smoothing of $sm_{VF} = 5 h^{-1} \text{Mpc}$. Differences between the mock catalogs are more pronounced than in the case with $sm_{VF} = 10 h^{-1} \text{Mpc}$.

Appendix D: Agora peculiar velocities

We found that the peculiar velocities in the AGORA simulation had an unexpected sign inversion. After performing several tests, we confirmed this issue and corrected it by flipping the sign of the velocities in our analysis. Part of those tests consisted on reproducing our findings using the halo lightcone files from Sato-Polito et al. (2023b), which were independently generated to replicate the AGORA lightcone—including the baryonic physics from the UNIVERSE MACHINE, as we also do—but specifically for Line-Intensity Mapping (LIM) studies. The resulting signals and conclusions using those data sets were consistent with the analyses presented in this work.

Appendix D.0.1: Tests

Void Size Function and Quadrupole In the AGORA simulation, voids in redshift space appear smaller and more numerous than in real space, in contrast to expectations from the MDPL2 simulation box and other established studies. Previous work shows that redshift-space distortions (RSD expansion) and the Alcock–Paczyński effect systematically increase void sizes

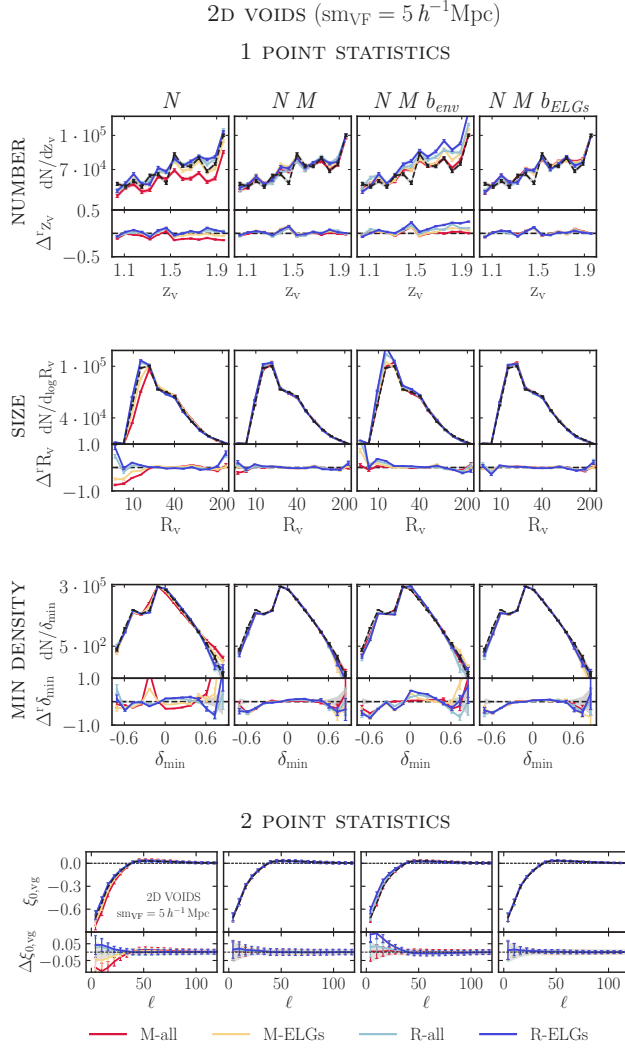


Fig. C.1: One- and two-point statistics for 2D voids with $sm_{VF} = 5$ Mpc/h. Each column represents a different mock catalog type. Different colors denote a different tracer bias. The bottom sub-panels display the residuals, defined as the relative difference with respect to the reference catalog.

along the line of sight (Ryden & Melott 1996; Lavaux & Wandelt 2012; Hamaus et al. 2015; Nadathur et al. 2019a; Correa et al. 2021b, 2022b). These distortions arise from universal physical mechanisms such as peculiar velocities and the cosmological metric, though their magnitude can depend on the simulation’s cosmology (Ω_m , h), redshift, and tracer properties (bias, density). However, an inversion where voids shrink at the considered scales and become more numerous is highly anomalous. Figure D.1 illustrates this behavior: the void size function, monopole, and quadrupole indicate that the original AGORA velocities produce voids with apparent matter inflows, which is physically inconsistent.

Angular Redshift Fluctuations Using angular redshift fluctuations Hernández-Monteagudo (2019), which are highly sensitive to radial peculiar velocities, we found that theoretical and measured angular power spectra only matched when the sign of v_{los} was inverted.

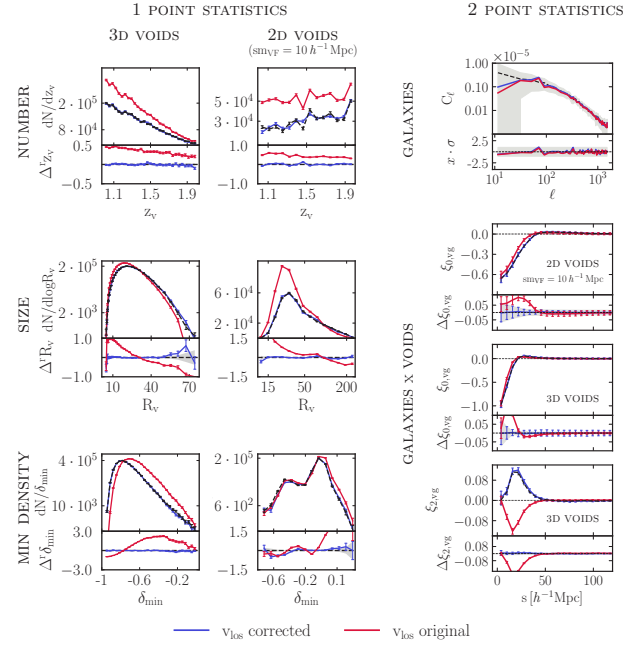


Fig. D.1: One- and two-point statistics for 3D and 2D voids ($sm_{VF} = 10$ Mpc/h) comparing AGORA velocities (original vs. sign-flipped). Residuals relative to *Roman* reference catalog.

Independent Cross-Check (SKYLINE) Using the Skyline code Sato-Polito et al. (2023b), an independent galaxy catalog generator compatible with AGORA’s CMB observables, we confirmed that flipping the line-of-sight velocities was necessary to correctly reproduce the kinematic Sunyaev-Zel’dovich (kSZ) signal of Omori (2024).